



# ThunderAgent: A Simple, Fast and Program-Aware Agentic Inference System

Hao Kang<sup>\*1</sup>, Ziyang Li<sup>\*2</sup>, Weili Xu<sup>\*3</sup>, Xinyu Yang<sup>\*4</sup>, Yinfang Chen<sup>3</sup>, Junxiong Wang<sup>5</sup>, Beidi Chen<sup>4</sup>, Tushar Krishna<sup>1</sup>, Chenfeng Xu<sup>5</sup>, and Simran Arora<sup>5</sup>

<sup>1</sup>Georgia Institute of Technology

<sup>2</sup>Individual Researcher

<sup>3</sup>University of Illinois Urbana-Champaign

<sup>4</sup>Carnegie Mellon University

<sup>5</sup>Together AI

 Code

 Blog

 Wiki

## Abstract

Large language models (LLMs) are now used to power complex multi-turn agentic workflows. Existing systems run agentic inference by loosely assembling isolated components: an LLM inference engine (e.g., vLLM) and a tool orchestrator (e.g., Kubernetes). Although agentic workflows involve multiple LLM and tool requests, these systems schedule and allocate resources separately on a per-request basis, without end-to-end knowledge of the workflow. This leads to sub-optimal management of KV cache and tool execution environments. To address the challenges, we propose THUNDERAGENT, a fast, simple, and program-aware agentic inference system. We first abstract agentic workflows as *LLM Programs*, enabling a unified view of heterogeneous resources, including KV caches, system states, and external tool assets such as disk memory and network ports. Built upon this abstraction, THUNDERAGENT introduces a program-aware scheduler and a tool resource manager designed to maximize KV cache hit rates, mitigate memory imbalances, and enable asynchronous environment preparation. Evaluations across coding, routing, and scientific discovery agents demonstrate that THUNDERAGENT achieves **1.5-3.6** $\times$  throughput improvements in serving, **1.8-3.9** $\times$  in RL rollout, and up to **4.2** $\times$  disk memory savings compared to state-of-the-art inference systems. To facilitate reproducibility and support future development, we open-source the system implementations of THUNDERAGENT at: <https://github.com/ThunderAgent-org/ThunderAgent>.

## 1 Introduction

Recent advances in language models have expanded their use beyond basic chatbots to complex agents [21, 27]. These agents address real-world problems in domains such as coding [8, 10] and computer-use [2, 25] by interleaving long reasoning with external tool calls (e.g., compilers, retrievers), often operating as autonomous systems that execute multi-step workflows without real-time human intervention. However, the throughput of modern inference systems degrades as the number of agentic requests being processed increases (Figure 1a). Meanwhile, rollout accounts for over **70%** of the total wall-clock time in reinforcement learning (RL) [5, 18].

As agentic workflows become increasingly autonomous at scale, overall system efficiency is governed by sustained throughput rather than tail latency, whereas human-in-the-loop applications are often dominated by user response times. Therefore, higher throughput directly reduces serving cost by amortizing hardware over more completed workflows. Moreover, in asynchronous RL, higher rollout throughput mitigates policy lag between the parameters used for data collection and those being updated. This allows the model to learn from data with reduced staleness, improving both convergence speed and final policy quality [5, 17, 18, 33].

<sup>\*</sup>Equal contribution. Correspond to [hkang342@gatech.edu](mailto:hkang342@gatech.edu)

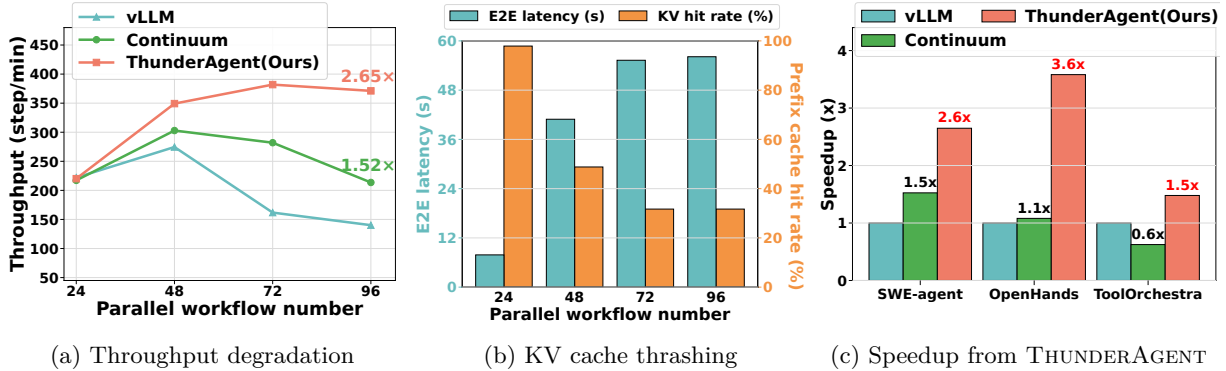


Figure 1: **Performance comparison of ThunderAgent against prior agent inference systems as the parallel workflow number (i.e., batch size) increases.** We evaluate the GLM-4.6 MoE model serving SWE-Agent on SWE-Bench Lite (Figures a and b) and SWE-Agent, OpenHands, and ToolOrchestra (Figure c) on an  $8 \times H100$  GPU cluster. Results show that: (a) Current inference systems fail to maintain high throughput at large batch sizes. (b) Throughput degradation is primarily caused by low KV cache hit rates, which increase end-to-end request latency. (c) THUNDERAGENT achieves high throughput compared to prior inference systems by reducing KV-cache thrashing and managing the lifecycle of tool execution resources.

However, current agentic inference systems provide sub-optimal throughput because they are loosely combined from isolated components: an off-the-shelf model inference engine (e.g., vLLM [11] or SGLang [34]) coupled with a general-purpose tool orchestrator (e.g., Kubernetes). While agentic workflows involve multiple turns of model and tool requests, these components schedule and allocate resources separately on a *per-request basis*, without end-to-end knowledge of the entire workflow. This design gives rise to three key challenges:

1. **KV cache thrashing.** Under memory pressure at high concurrency, request-aware systems reactively evict the KV cache of programs in their tool-execution intervals to make room for decode requests of other concurrent programs, without foresight into future reuse in the agent workflow. Thus when the tool call completes, the system needs to rerun prefill to recover its whole interaction history. The re-prefill cost increases the average end-to-end latency of agent workflows by up to  $7.14 \times$  (see Figure 1b) and decreases throughput.
2. **Cross-node memory imbalance.** The request-aware engines suffer from imbalanced utilization in multi-node inference setups. Existing engines pin all requests from the same agentic workflow to a fixed node to maximize the KV cache hit rate. However, as context lengths scale rapidly and unpredictably in agent workflows, some nodes reach capacity while others remain underutilized under this routing policy.
3. **Tool lifecycle obliviousness.** The request-aware orchestrators struggle to decide when to release and prepare resources and environments required for tool execution. Thus, unused sandboxes and API servers continue to occupy critical disk space and network ports, leading to cumulative resource exhaustion and system failures. Meanwhile, agentic workflows have to wait for extremely long setup time before reasoning.

This work introduces THUNDERAGENT, an agentic inference system that adopts an end-to-end view of agentic workflows to enable high-throughput agentic serving and RL rollout. Our specific contributions are:

1. **Program abstraction:** We abstract agent workflow as *agentic programs*. An agentic program is a first-class scheduling unit that persists across multiple model invocations and tool executions, exposing semantic state to the runtime. A program tracks metadata for the workflow’s identifier, execution phase (i.e., reasoning or acting), scheduling status, total tokens, and tool resources. This abstraction decouples scheduling from execution backends (e.g., vLLM/SGLang/TensorRT-LLM), enabling seamless integration of new workflows.
2. **Program-aware scheduler:** Based on the program abstraction, we cast agentic inference scheduling as a constrained optimization problem to minimize the recomputation and caching overheads, and maximize prefilling and decoding throughput, subject to GPU memory capacity. We introduce two key mechanisms:
  - (a) **State-aware pausing:** If the execution backend experiences memory pressure, we selectively pause

workflows that are currently in the acting state with tool call. This design helps preserve memory for programs that are in the reasoning state and eliminate arbitrary, sub-optimal KV cache eviction.

- (b) **Dynamic migration:** We migrate agent programs across data parallel (DP) GPU nodes to mitigate memory imbalance. We accomplish this by enabling all DP nodes share a global program-aware waiting queue, rather than enforcing that requests from a program are always sent to the same node.

3. **Program-aware tool resource management:** In long-horizon agentic workloads, tool environments are persistent resources whose mismanagement directly limits sustained throughput. By tracking execution dependencies, THUNDERAGENT overlaps I/O-intensive environment initialization with LLM reasoning. For completed programs, we implement a lifecycle-aware garbage collector that leverages program termination signals to reclaim tool resources such as Docker sandboxes and network ports. Consequently, this prevents accumulated resource leakage and ensures sustained high-throughput agentic inference in THUNDERAGENT.

The above contributions cannot be achieved within request-aware inference engines. Without an explicit representation of program states and workflow dependencies, request-aware schedulers cannot distinguish temporary tool waits from termination or coordinate GPU memory with program-level resource scheduling.

We evaluate THUNDERAGENT across diverse agentic workloads. For **servicing**, we evaluate the ToolOrchestra [19] as routing agent on HLE-Bench [16], SWE-Agent [28] and OpenHands [24] as coding agent on SWE-bench [10], and OpenHands as scientific discovery agent on ScienceAgentBench [4], achieving **1.48–3.58×** throughput improvements as illustrated in Figure 1c. For **RL rollouts**, we further test the coding agents on distributed GPU nodes, achieving **1.79–3.92×** improvements compared with prior SOTA systems.

Beyond these results, we evaluate THUNDERAGENT under common large-scale deployment settings. As detailed in the appendix, THUNDERAGENT’s throughput scales near-linearly with multiple worker replicas on up to 64 H100 GPUs (Section A.3), and remains effective when combined with KV-cache offloading (Section A.4). THUNDERAGENT has been adopted by open-source frameworks such as SkyRL and NVIDIA Dynamo (Section A.6).

## 2 Background

In this section, we provide background on the properties and existing approaches to support agentic inference.

### 2.1 System Properties of Current Agentic Workflows

Current agentic workflows alternate between reasoning and acting during generation. Formally, at each step  $t$ , the agent receives an observation  $o_t \in \mathcal{O}$  and produces an emission  $e_t = (\ell_t, a_t) \in \mathcal{L} \times \mathcal{A}$ , where  $\ell_t$  denotes a thought and  $a_t$  represents an action. We define the cumulative context at step  $t$  as  $c_t = (o_1, e_1, \dots, o_t)$ , which captures the interaction history of agentic workflows. Conditioned on  $c_t$ ,  $e_t$  is sampled from a policy  $\pi(e_t|c_t)$ .

This workflow keeps two persistent states: (i) *GPU Memory*, where the KV cache of  $c_t$  serves as the workflow’s memory. As the trace grows incrementally,  $c_{t+1}$  extends  $c_t$  as a prefix, enabling theoretical near-complete KV cache reuse rates across steps. (ii) *Tool Environment*, where external resources (e.g., sandboxes) initialized at  $t = 1$  must remain consistent and accessible throughout the execution.

These stateful dependencies necessitate a *program-level* view of agentic inference trajectories, thereby enabling to system to coordinate heterogeneous resources and manage state across long-running workflows. However, existing inference systems treat each thought  $\ell_t$  and action  $a_t$  as an independent, stateless request.

### 2.2 Existing Agentic Inference Systems

Prior work focuses on optimizing the individual components in agentic inference, including the LLM inference engine or tool orchestrator (Section A.1, Section A.2), but there are very few works that provide end-to-end optimization for agentic workflows across GPU, CPU, and remote resources.

Autellix models multi-turn agentic workflows as **GPU-only programs** and tracks the accumulated GPU execution time in a central process table [14]. However, it ignores workflow locality, allowing concurrent workflows to aggressively evict other’s KV cache, triggering **KV cache thrashing** under heavy workloads.

Continuum is another recent serving system designed for multi-turn agentic workflows [12]. It employs a time-to-live (TTL) mechanism to pin KV caches in HBM, thereby mitigating context thrashing during tool execution. However, it fails to solve the KV cache eviction problem. The first reason is that most tools take

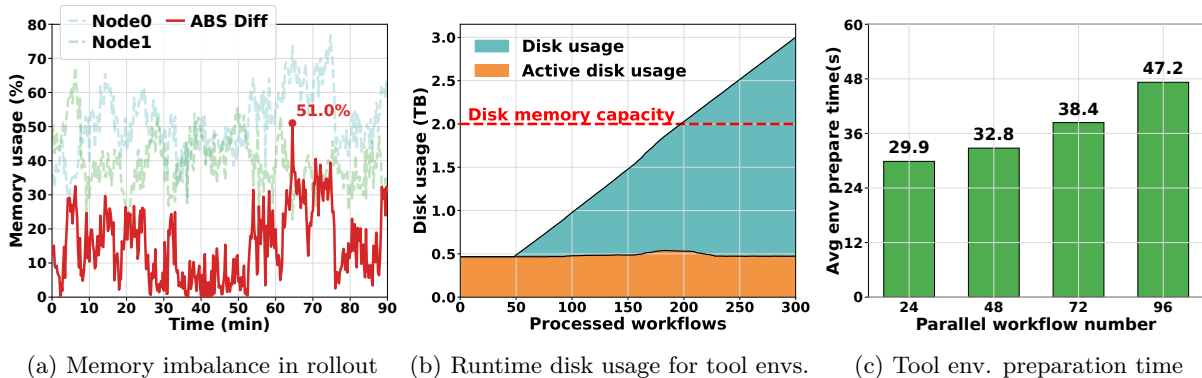


Figure 2: **Demonstrations of the memory imbalance and tool resource management problems for current agentic inference systems.** We evaluate vLLM + Kubernetes on OpenHands RL rollout using the GLM 4.6 model on SWEBench-Lite with two 8×H100 GPU Nodes. The observations show: (a) Max memory imbalance can achieve 51% on 90 min rollout tests when applying vLLM KV-aware router. (b) Failure to garbage collect tool execution environments gradually causes resource usage to exceed system capacity. (c) Average tool execution environment preparation time grows fast as parallel workflow number increases.

an **unpredictable** amount of time (e.g. remote model APIs in ToolOrchestra [19], compilers in code agents, and web applications for computer use agents [36]). Such unpredictable tools trigger severe thrashing as well as stranded KV cache memory in Continuum due to incorrect TTL estimates. Moreover, once the decoding memory of the running workflow surpasses the GPU limit, the system preempts and evicts pinned KV cache as well. This leads to unavoidable thrashing and corresponding throughput degradation shown in Figure 1a.

These limitations underscore the need for a simple and fast system for agentic inference. We envision such a system as a program-aware scheduling layer for emerging agentic inference systems (e.g., Zhang et al. [32]).

### 3 Challenges in Existing Agentic Inference Systems

This section profiles vLLM combined with Kubernetes as a representative baseline for multi-turn agentic inference, and synthesize its key inefficiencies. Notably, the identified limitations cannot be solved by replacing the inference engine, but rather require new program-aware abstractions. By default, we use GLM 4.6 model for OpenHands RL rollout on two 8×H100 GPU nodes.

#### 3.1 KV Cache Thrashing

Agentic workflows exhibit a high theoretical KV cache reuse rate during their execution. However, in existing LLM serving systems, each step is served as an independent and stateless request. Under high concurrency, this request-level scheduling causes KV cache to be frequently evicted during tool execution to accommodate newly arriving requests, resulting in repeated eviction and re-prepare, which we refer to as **KV cache thrashing**.

As shown in Figure 1b, this thrashing intensifies as the number of parallel workflows increases. The resulting degradation in cache hit rates triggers frequent and costly re-prepare, where the prefix must be recomputed upon tool completion. This redundancy significantly increases the end-to-end latency of each request by up to **7.14×** compared to a non-thrashing setting, leading to severe throughput degradation.

#### 3.2 Cross-Node Memory Imbalance

Current policies for routing requests across worker replicas are also sub-optimal. Existing multi-turn schedulers [22, 34] greedily assign requests to the target with the highest KV-cache locality in order to maximize cache reuse. However, this policy ignores the fact that the memory load can become imbalanced across nodes. For instance, the KV-aware router in vLLM [22] sends all requests from the same agentic workflow to the same node. Since different workflows can exhibit highly heterogeneous KV footprints and execution lifetimes, this policy often results in severe memory imbalance across nodes, with some nodes

are overloaded while others remain lightly utilized. Similarly, the cache-aware router in SGLang routes via a router-side radix tree that approximates worker KV state. Under high agentic concurrency, worker-side evictions from KV thrashing leave this tree stale, yielding both poor cache reuse and cross-node imbalance.

As shown in Figure 2a, during a 90 minute snapshot of agentic RL rollout, the memory usage between two DP nodes diverges by **more than 20% for over 37 minutes, reaching a peak imbalance of 51%**.

### 3.3 Tool Lifecycle Obliviousness

Current agentic inference systems do not synchronize the external tool orchestrator’s lifecycle with the LLM inference engine, resulting in silent resource wastage and latency overhead on the tool orchestrator side.

**Resource leakage and unused sandboxes.** Figure 2b showcases that the total disk space consumption increases linearly with the number of processed workflows, eventually exceeding system capacity. This is because unused resources (e.g., Docker images of finished workloads) are not reclaimed when workflows complete. This inefficient garbage collection leads to fatal system instabilities for long-running agentic inference workloads.

**Costly environment preparation.** We observed that most agentic workloads need to prepare environments before initiating the multi-turn trajectory. For example, coding agents need to pull dockers, install related packages and build repositories. Furthermore, this preparation time is costly and increases with the parallel workload number, as shown in Figure 2c. If the LLM inference engine needs to wait until the environments are fully prepared, this overhead will extend the end-to-end latency of the inference system.

## 4 ThunderAgent: A Program-Aware Agentic Inference System

With all findings in Section 3, we present THUNDERAGENT, a program-aware system for high throughput agentic inference. We model the Agentic Program in Section 4.1, which serves as our primary abstraction for scheduling. Section 4.2 formalizes a cost model to guide our system design. Built upon these foundations, we detail our KV cache scheduling policy in Section 4.3 and tool resource management strategy in Section 4.4.

Table 1: **Summary of Notations for agentic programs.** Each program instance is characterized by its identity, execution phase, tool environments, resource footprint, and scheduling state.

Notation	Description
$P$	Agentic program instance
$ID$	Unique global identifier for the program
$c$	Number of tokens in the context
$\mathcal{T}$	Set of tool environments required by the program
$\mathcal{L}$	Backend placement for cache affinity
$\tau$	Execution phase: Reasoning ( <b>R</b> ), Acting ( <b>A</b> )
$s$	Scheduling status: {Active, Paused, Terminated}

### 4.1 Program Abstraction

The **Agentic Program** serves as a fundamental abstraction that encapsulates both the logical execution flow and the system-level dependencies of agentic workflows. Formally, we define an agentic program  $P$  as a tuple:

$$P = \langle ID, c, \mathcal{T}, \mathcal{L}, \tau, s \rangle, \tag{1}$$

where  $ID$  represents the unique global identifier.  $c$  denotes the number of tokens in the context, corresponding to the KV cache memory footprint during active execution.  $\mathcal{T}$  tracks the set of tool environments used by the program, enabling garbage collection when no program requires them further.  $\mathcal{L}$ ,  $\tau$ , and  $s$  denote the node placement, execution phase, and scheduling status, respectively, facilitating program-level KV cache thrashing reduction and cross-node transferring. A metadata example is demonstrated on the right side of Figure 3.

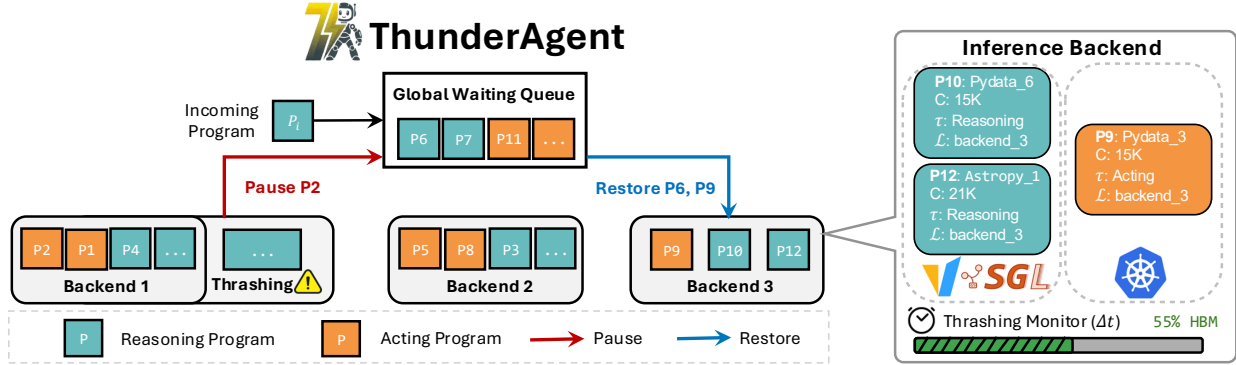


Figure 3: **An Overview of ThunderAgent.** We show the transition between scheduling states and memory management. THUNDERAGENT queries the state of each data parallel backend periodically every  $\Delta t$  time. Here, Backend #1 triggers thrashing, while Backend #3 is underutilized. The global waiting queue shared by all Backends then pauses and collects acting Program #2 back to the queue while releasing reasoning Program #6 and #9, to stop the KV-cache thrashing in Backend #1 and reduce memory imbalance of Backend #3.

THUNDERAGENT directly wraps existing LLM engines and tool orchestrators by interfacing with OpenAI-style endpoints. Program IDs allow the system to distinguish requests from different agentic workflows. We elaborate on the simplicity of integrating THUNDERAGENT with existing inference services in Appendix B.

## 4.2 Cost Model

During multi-turn agentic inference, only the resources used for active prefilling and decoding contribute to the system’s effective throughput, while re-computation, used capacity, and idle caching constitute resource waste. We encompass this in a cost model for GPU resource consumption, which isolates effective costs from non-productive usage. We adopt the Space-Time Product (STP) [1] as our primary metric, defined as the integral of the memory footprint over processing time. The STP cost during a process phase is formalized as:

$$\text{Cost}_x = \int_0^{t_x} M_x(t) dt, \quad (2)$$

where  $t_x$  is the duration of process  $x$  (e.g., prefill). Since memory usage  $M_x(t)$  can be directly quantified by the KV cache token count used in LLMs, we define our cost model as the integral of token count over time.

The total cost of agentic inference comprises five distinct components: decoding, prefilling, recomputation, unused capacity, and idle caching. We explicitly distinguish incremental prefilling for tool execution results from recomputation over historical interactions, with the latter leading to significantly higher cost due to re-computing evicted KV cache over the full context. Formally, this yields the following cost decomposition:

$$\text{Cost}_{\text{total}} \approx \text{Cost}_{\text{decode}} + \text{Cost}_{\text{prefill}} + \text{Cost}_{\text{recompute}} + \text{Cost}_{\text{unused}} + \text{Cost}_{\text{caching}} \quad (3)$$

In this decomposition,  $\text{Cost}_{\text{decode}}$  and  $\text{Cost}_{\text{prefill}}$  represents the effective work that contributes to inference throughput. The remaining terms are wasted system overheads:  $\text{Cost}_{\text{recompute}}$  stems from KV cache thrashing (Section 3.1);  $\text{Cost}_{\text{unused}}$  reflects memory imbalance across data parallel (DP) inference backend replicas (Section 3.2); and  $\text{Cost}_{\text{caching}}$  accumulates while holding memory during external tool execution (Section 3.3).

## 4.3 Scheduling Policy

Based on the cost model above, the optimization target of our scheduling policy is to minimize the non-productive overhead components:  $\text{Cost}_{\text{recompute}}$ ,  $\text{Cost}_{\text{unused}}$ , and  $\text{Cost}_{\text{caching}}$ , thereby maximizing throughput.

### 4.3.1 Reducing Recomputation and Caching Costs via Program-Aware Waiting Queue

As identified in Section 3.1 and Figure 1b, KV cache thrashing serves as the primary bottleneck for throughput degradation. To address this limitation, the system must minimize  $\text{Cost}_{\text{recompute}}$  by explicitly controlling

the number of active programs. THUNDERAGENT achieves this by introducing a program-aware waiting queue. Our system utilizes this queue to schedule program execution, determining which program should be executed in GPU versus which should be swapped out based on their token length  $c$  and execution phase  $\tau$ . Here, we formalize the scheduler behavior using two primitive operations: **Restore** and **Pause**, as follows.

- **Restore.** This operation admits a program into active execution. Given a program  $P = \langle ID, c, \mathcal{T}, \mathcal{L}, \tau, s \rangle$  with  $s = \text{Paused}$  and  $\mathcal{L} = \emptyset$ ,  $\text{Restore}(P)$  assigns  $P$  to a backend  $\mathcal{L}'$  with available capacity and updates

$$P \leftarrow \langle ID, c, \mathcal{T}, \mathcal{L}', \tau, \text{Active} \rangle, \quad (4)$$

- **Pause.** This operation removes a program from active execution. Given a program  $P = \langle ID, c, \mathcal{T}, \mathcal{L}, \tau, s \rangle$  with  $s = \text{Active}$ ,  $\text{Pause}(P)$  unbinds  $P$  from its backend, releases its KV cache for preemption, and updates

$$P \leftarrow \langle ID, c, \mathcal{T}, \emptyset, \tau, \text{Paused} \rangle. \quad (5)$$

Building on these two operations, we next introduce our scheduling policy to minimize KV cache thrashing.

**Periodic thrashing detection.** The program abstraction in [Section 4.1](#) provides us with the KV cache size of acting programs. Notably, this is unavailable in request-level systems (as in [Section 3](#)). We define the thrashing condition for a DP backend  $\mathcal{L}$  as the state where program memory demand exceeds total capacity:

$$C_{\text{total}} < \sum_{p \in \mathcal{L}} c_p \quad (6)$$

where  $C_{\text{total}}$  denotes the fixed token capacity of the KV cache pool for backend  $\mathcal{L}$ . During decoding, the context length  $c_p$  of agentic workflows grows rapidly, which can trigger memory thrashing *mid-execution* even without of new arrivals. Unlike baseline schedulers (e.g., Continuum) that only perform checks on whether to admit a workflow upon its arrival, we implement a **periodic monitor** that evaluates the memory usage at fixed intervals  $\Delta t$ , allowing preemptive detection and mitigation of memory pressure caused by context growth.

When KV cache thrashing is imminent, THUNDERAGENT invokes **Pause** operation to suspend active programs and free memory size  $\Delta C = \sum_{p \in \mathcal{L}} c_p - \lambda_{\text{max}} \cdot C_{\text{total}}$  until the total memory usage falls below the limit  $\lambda_{\text{max}} \cdot C_{\text{total}}$ . Conversely, when the backend has available space, meaning  $\sum_{p \in \mathcal{L}} c_p < \lambda_{\text{min}} \cdot C_{\text{total}}$ , THUNDERAGENT restores paused programs from the waiting queue via **Restore**, ensuring that the restored program keeps the total memory below  $\lambda_{\text{max}} \cdot C_{\text{total}}$ . Here,  $\lambda_{\text{max}}$  and  $\lambda_{\text{min}}$  denote the high- and low-watermarks of memory usage, respectively, together forming a hysteresis window that stabilizes our scheduling. In practice, we set both value to be 1, as the shared prompt across programs implicitly reserves sufficient memory buffer.

With this program-level periodic capacity check, THUNDERAGENT can guarantee that there will be no KV cache thrashing by reserving memory for active programs during the acting phase. However, the tradeoff is that when programs engage in long-running tool execution, the GPU memory occupied by acting programs is idle. To balance the cost of caching against recomputation, we incorporate a time-decay mechanism into the thrashing check that progressively discounts the effective weight of acting programs' tokens. This allows the scheduler to evict long-idling caching when memory pressure rises, rather than holding them indefinitely:

$$C_{\text{total}} < \sum_{p \in \mathcal{L}, \tau = \mathbf{R}} c_p + \sum_{q \in \mathcal{L}, \tau = \mathbf{A}} c_q \times f(t_q) \quad (7)$$

Specifically,  $t_q$  is the tool execution time of program  $q$  in the current step.  $f(t)$  is a time-decay function designed to balance  $\text{Cost}_{\text{caching}}$  and  $\text{Cost}_{\text{recompute}}$ . Note that this decayed check governs both **Pause** and **Restore**: shrinking an idle program's weight admits more reasoning programs, whose decoding then raises pressure and triggers the eviction of its KV cache. By dynamically lowering the effective memory priority of acting programs over time,  $f(t)$  encourages the scheduler to evict caches that remain idle. In [Section F.1](#), we prove that when tool execution latencies satisfy the memoryless property (i.e., the remaining execution time is independent of the elapsed duration), exponential decay is the only admissible form of  $f(t)$ .

**Minimizing  $\text{Cost}_{\text{recompute}}$  via Shortest-First Eviction.** With the eviction and restoration conditions above, the remaining question in handling thrashing is to determine which subset of active programs to pause such that the recomputation cost is minimized. In this paragraph, we demonstrate that evicting programs with the smallest KV cache size yields the optimal solution, with a detailed proof provided in [Section F.2](#).

**Lemma 4.1** (Quadratic Recomputation Cost). *Given a program  $P_i$  with context length  $c_i$ , the recomputation cost incurred by refilling its KV cache scales quadratically with  $c_i$ , i.e.,*

$$\text{Cost}_{\text{recompute}} = \int_0^{t_{\text{recompute}}} c_i(t) dt \propto c_i^2. \quad (8)$$

**Definition 4.1** (Eviction Optimization Problem). Based on [Lemma 4.1](#), given a required memory release  $\Delta C$ , the scheduler aims to select a subset  $S$  of programs to evict such that the released capacity satisfies the constraint while minimizing the total recomputation cost. This optimization problem is formulated as follows:

$$\min_S \sum_{i \in S} c_i^2 \quad \text{s.t.} \quad \sum_{i \in S} c_i \geq \Delta C. \quad (9)$$

The objective is strictly minimized by selecting smaller  $c_i$ . Thus, THUNDERAGENT’s strategy is to greedily pause and evict programs with the **shortest context lengths**. We defer the formal proof to [Appendix F.3](#). Based on these analyses, we employ the following scores for restoring and pausing a program in our scheduler:

$$S_{\text{restore}}(P) = \frac{1}{c_P} + \mathbb{I}(\tau = \mathbf{R}) \quad (10)$$

$$S_{\text{pause}}(P) = \frac{1}{c_P} + \mathbb{I}(\tau = \mathbf{A}) \quad (11)$$

where the indicator function  $\mathbb{I}(\cdot)$  enforces strict prioritization of the program’s execution state ( $\tau$ ) over context length. Both mechanisms follow the **shortest-first** policy to minimize recomputation cost. However, the state indicator  $\mathbb{I}$  ensures that the scheduler prioritizes pausing Acting programs, thereby minimizing  $\text{Cost}_{\text{caching}}$  by reclaiming cached memory, while prioritizing restore Reasoning programs to maximize  $\text{Cost}_{\text{decode}} + \text{Cost}_{\text{prefill}}$ .

### 4.3.2 Reducing Memory Imbalance via Global Program-Aware Waiting Queue

[Section 3.1](#) and [Figure 2a](#) highlight that memory imbalance across nodes introduces significant  $\text{Cost}_{\text{unused}}$ , leading to unnecessary program pausing despite sufficient memory capacity from other nodes. To this end, THUNDERAGENT unify waiting queues of all backend replicas into a **global program-aware waiting queue**.

The key motivation of this design is that  $\text{Cost}_{\text{unused}}$  arises only when paused programs remain in the waiting queue while some replicas have idle memory. Moreover, once a program is paused, its KV cache is assumed to be evicted, making its recomputation cost node-agnostic. This allows us to improve cross-node memory balance without sacrificing KV cache locality. The restore policy aligns with load balancing rather than strict KV-aware routing, enabling paused programs to be resumed on the worker replica with available memory capacity. As a result, the global queue bounds the unused cost such that  $C_{\text{unused}} < c_{\text{min}} \cdot \Delta t^1$  for every node in the period of  $\Delta t$ , where  $c_{\text{min}}$  represents the minimum token length among paused programs. An overview of the scheduling policy and the global waiting queue in THUNDERAGENT is presented in [Figure 3](#).

## 4.4 Tool Resource Management

Next, THUNDERAGENT mitigates the resource leakage and environment setup overheads detailed in [Section 3.3](#).

**Hook-based garbage collection.** We implement lifecycle hooks that strictly couple the persistence of tool resources with the agentic program’s scheduling status  $s$ . When a program is *Terminated*, the collector triggers an immediate teardown sequence, systematically reclaiming sandboxes, network sockets, and compute slots. The active disk usage in [Figure 2b](#) shows that our resource management policy effectively prevents the accumulation of excessive resources and maintains near-constant disk memory consumption over time.

<sup>1</sup>Since  $\Delta t$  is much smaller than a program’s lifetime, we ignore the impact of terminated programs within a single interval.

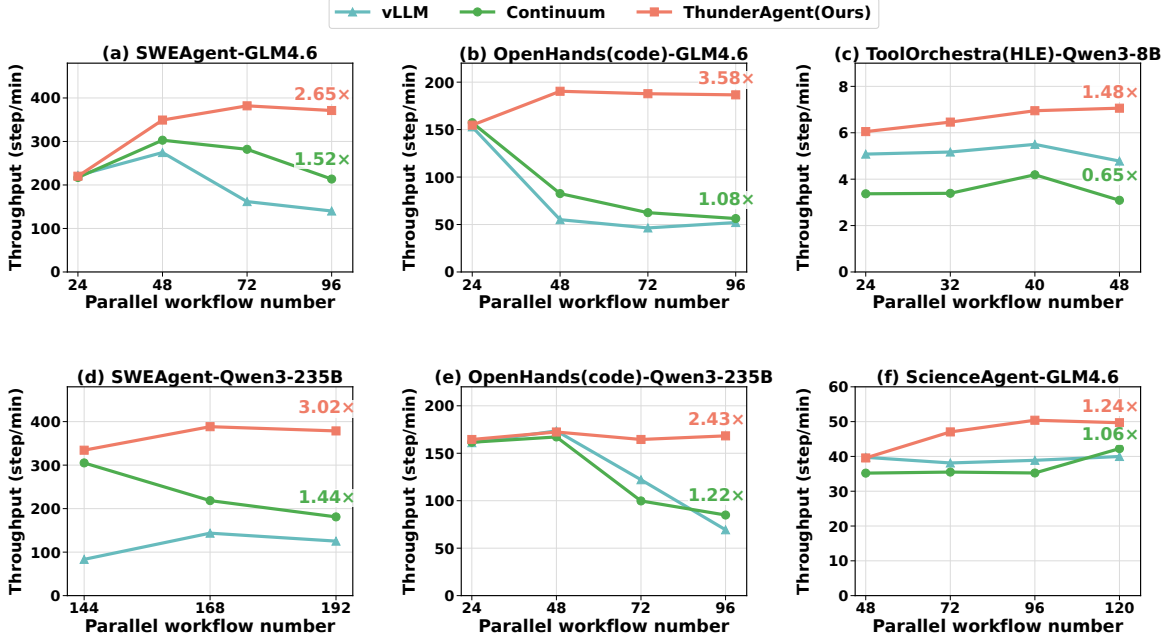


Figure 4: **Serving Evaluation Results.** THUNDERAGENT outperforms vLLM and Continuum across three models, four agentic workflows, and three datasets. For workflows with predictable tool call times (a, b, d, e), THUNDERAGENT outperforms vLLM and Continuum up to 2.43-3.56 $\times$ . For workflows exhibit stochastic tool execution time (c, f), THUNDERAGENT still achieves the best throughput performance.

**Asynchronous environment preparation.** The latency involved in initializing a tool execution environment (e.g., starting a Docker container and installing dependencies) can be a bottleneck. To address this, THUNDERAGENT monitors the global waiting queue; when a high-priority program (high  $S_{\text{restore}}$ ) approaches the restore threshold, the system asynchronously restores its execution environment before the GPU memory is allocated. This technique effectively **hides the initialization overhead**, significantly reducing end-to-end latency for tool-call heavy workloads like coding agents and science agents, as demonstrated in Figure 2c.

## 5 Experiments

In this section, we evaluate THUNDERAGENT on diverse agentic workflows, including coding, routing, and scientific research agents, and RL rollout across multiple hardware configurations ranging from RTX5090 to H100 clusters. Furthermore, we conduct extensive ablation studies to breakdown the end-to-end system runtime and to describe the system’s sensitivity to the scheduler’s hyperparameters,  $\Delta t$  and  $f(t)$ , in Section 5.4.

### 5.1 Experimental setup

**Benchmarks and workflows.** We evaluate THUNDERAGENT against diverse benchmarks and workloads:

1. **Coding agent serving.** We deploy **OpenHands** and **mini-SWEAgent** on the SWEBench-Lite [10]. OpenHands represents a **heavy-initialization workflow** with an average disk footprint exceeding 10GB per sandbox, while mini-SWEAgent is a **lightweight workflow** with a minimal footprint (2GB per sandbox).
2. **General agent serving.** We apply ToolOrchestra on HLE [16] and OpenHands on ScienceAgentBench [4]. These workloads involve variable latencies driven by external API calls and complex scientific simulations.
3. **RL rollout.** We apply the same models, workflows, and samples for RL rollout on two 8 $\times$  H100 nodes.

**Models and deployments.** We employ GLM-4.6 (355B) [21] and Qwen-3 (235B) [27] using both OpenHands [24] and mini-SWEAgent [28] frameworks. Models are quantized to FP8 with Tensor Parallelism (TP8) on 8 $\times$ H100 nodes. For ToolOrchestra [19], we use Qwen3-8B with FP16 precision hosted on one RTX 5090.

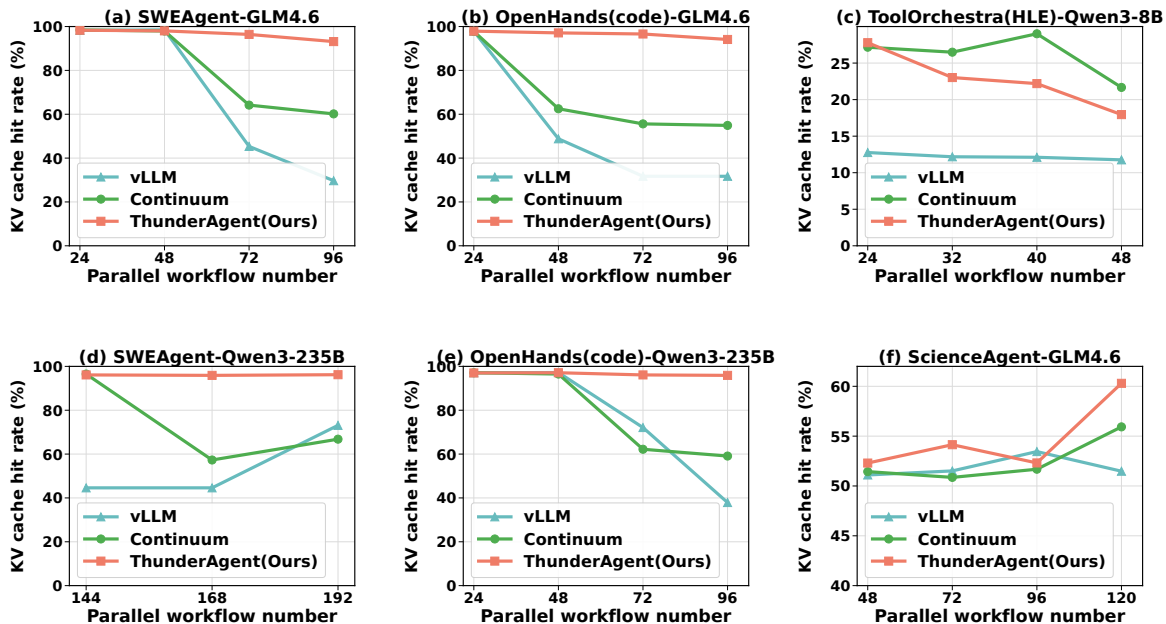


Figure 5: **KV Cache Hit Rate.** THUNDERAGENT achieves near-optimal KV hit rate with predictable tool call time (a, b, d, e), while dynamically trading KV cache hit rate for better compute utility when serving workflows with stochastic tool execution time (c, f).

We deploy the LLM inference engine and Docker at different clusters. The LLM inference engine runs on GPU clusters hosting the models, while agent Docker environments are offloaded to a dedicated CPU cluster.

**ThunderAgent configuration.** We configure THUNDERAGENT with hyperparameters  $\Delta t = 5$  and priority decay  $f(t) = 2^{-t}$ , defined in Section 4.3. vLLM is employed as our LLM inference engine. We use steps per minute as our throughput metric, where one step includes a reasoning and acting period of the workflow.

**Baseline techniques.** We compare against state-of-the-art systems with different scheduling paradigms:

- **vLLM (Inference):** A widely adopted, request-aware LLM inference engine that serves as a stateless baseline for inference performance, without incorporating any agent- or program-specific awareness.
- **Continuum (Inference):** The current SOTA system for multi-turn agentic workflows. It mitigates KV cache thrashing by predicting tool execution durations and pinning KV cache to HBM correspondingly.
- **vLLM + SGLang Gateway (Distributed Rollout):** The leading solution for large-scale distributed RL rollout. SGLang Gateway optimizes distributed inference by enhancing cross-node memory balancing and KV cache hit rates, making this combination a strong baseline for the distributed RL rollout setting.

## 5.2 Serving Evaluation Results

**High throughput under high concurrency.** Figure 4 showcase that THUNDERAGENT demonstrates superior throughput at high concurrency levels (e.g., 96 parallel programs), achieving a  $1.48\text{--}3.58\times$  speedup over vLLM and  $1.17\text{--}3.31\times$  speedup over Continuum across diverse base models and datasets. This gain rises from our program-aware scheduler, which maintains a near-optimal KV cache hit rate ( $\approx 100\%$  for Mini-SWE-Bench and OpenHands, see Figure 5 a, b, d, e) and enables the asynchronous preparation of environments. In contrast, Continuum suffers from performance degradation under high concurrency. As shown in Figure 5, its KV cache hit rate drops significantly from  $>90\%$  to  $\approx 60\%$ . This is because Continuum suffers from KV cache eviction among requests in different programs when no enough memory is available for ongoing requests’ decoding. As a result, active programs compete for limited memory and trigger thrashing.

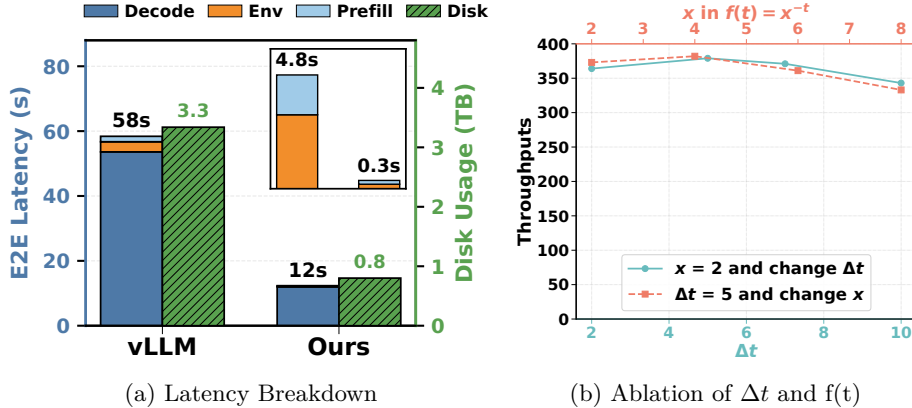


Figure 6: Ablation study of end-to-end latency breakdown and parameter sensitivity of THUNDERAGENT.

**Robustness performance to high concurrency.** THUNDERAGENT maintains maximum achievable throughput even as the parallel workflow number scales beyond the GPU memory limit. As shown in Figure 4, THUNDERAGENT ensures that throughput remains stable with the number of parallel workflows, whereas baseline systems suffer from severe throughput collapse once the workload exceeds memory limits. In practice, determining the optimal parallel workflow number to maximize utilization with limited KV cache thrashing and caching cost is infeasible due to the stochastic nature of agent environments and tool execution durations. THUNDERAGENT addresses this by automatically adapting to the maximum available capacity without manual tuning, a capability critical for robust real-world deployments.

**Robustness across deterministic and stochastic tool executions.** THUNDERAGENT outperforms baselines not only in workflows with deterministic tool patterns (Figure 4 a, b, d, e) but also under highly stochastic conditions (Figure 4 c, f). This comes from our dynamic program-aware waiting queue policy. vLLM’s request-aware scheduler typically lacks reserved memory for acting programs, forcing frequent re-computation. Conversely, Continuum statically reserves memory for all paused programs and miscalculates the tool execution time. These lead to expensive  $\text{Cost}_{\text{recompute}}$  or  $\text{Cost}_{\text{caching}}$  during long, unpredictable tool calls. THUNDERAGENT balances them via a time-decay function  $f(t)$ , which prioritizes retaining KV cache for programs with short tool calls while preemptively pausing programs with long tool execution time to prevent memory waste. As shown in Figure 5 (right), although THUNDERAGENT exhibits a lower KV cache hit rate than Continuum in stochastic settings, it achieves higher throughput by ensuring active GPU utilization.

### 5.3 Rollout Evaluation Results

We evaluate RL rollout using GLM-4.6 on a two-node H100 cluster. Table 2 shows that THUNDERAGENT can maintain effective scalability, achieving a  $1.79\text{--}3.92\times$  throughput increase over the vLLM + Gateway baseline, making it highly efficient for memory-intensive distributed RL workloads.

Table 2: GLM-4.6 rollout ( $N = 144$ ) on  $2\times\text{H100}$  nodes.

Workflow	Serving System	Throughput
mini-SWEAgent	vLLM + Gateway	375.4
mini-SWEAgent	THUNDERAGENT	671.8 ( $1.79\times$ )
OpenHands	vLLM + Gateway	69.1
OpenHands	THUNDERAGENT	270.8 ( $3.92\times$ )

### 5.4 Ablation Study

**End-to-end latency breakdown.** Figure 6a decomposes the average end-to-end latency for OpenHands rollouts. The throughput gain stems primarily from reductions in **prefill and decode latency**. Moreover, the tool resource management policy (Section 4.4) contributes approximately 10% to the latency improvement while providing  $4.2\times$  disk memory savings. Per-step end-to-end latency are further discussed in Appendix E.

**Ablation on  $\Delta t$  and  $f(t)$ .** We study the sensitivity of detecting period  $\Delta t$  and decaying function  $f(t) = x^{-t}$ . [Figure 6b](#) shows THUNDERAGENT offline serving mini-SWEAgent with GLM4.6 as base model on a single H100 node. We observe that THUNDERAGENT maintains high throughput under different parameter settings, demonstrating the robustness of our method. Further increasing  $\Delta t$  might decrease the KV cache hit rate and thereby reduce throughput because thrashing might occur in the middle of detecting. Also, increasing  $x$  in  $f(t)$  allows more aggressive eviction of acting programs, which trade recomputation costs to reduce caching costs. This reduces throughput as acting programs with short tool execution time are prematurely evicted.

## 6 Conclusion

We introduce THUNDERAGENT, a fast and simple agentic system built on a program-level abstraction that tracks metadata throughout the entire lifecycle of each agentic workflow. THUNDERAGENT leverages the program abstraction for runtime scheduling and resource management. Specifically, THUNDERAGENT dynamically schedules program execution across GPU nodes to mitigate KV cache thrashing and memory imbalance, while managing tool resources to prevent resource leakage. Experimental results showcase that THUNDERAGENT outperforms previous systems by **1.48–3.58** $\times$  for serving and **1.79–3.92** $\times$  for RL rollouts.

## Acknowledgements

We are grateful to Together AI for making this work possible. We thank Ben Athiwaratkun and Ce Zhang for assistance in developing the multi-backend scheduler. We thank Wenyi Hong and Luke Huang for helpful feedback and discussions during this work.

## Impact Statement

This paper presents work whose goal is to advance the field of Machine Learning Systems, specifically by optimizing the execution efficiency of agentic workflows. By significantly reducing the memory footprint and hardware requirements for maintaining agent inference and RL rollout, our method improves the **cost-efficiency** and **energy sustainability** of large-scale agent serving.

Our approach enables the training and inference of larger models and more complex environments on limited hardware resources. This efficiency helps companies and individuals to advanced agent research, allowing a broader range of institutions and practitioners to engage in high-fidelity simulations without necessitating prohibitive computational investments. While increasing system throughput could theoretically accelerate both positive and negative applications of autonomous agents, our work primarily targets infrastructure optimization, which is essential for the scalable and sustainable development of the field.

## References

- [1] L. A. Belady. A study of replacement algorithms for a virtual-storage computer. *IBM Systems Journal*, 5(2):78–101, 1966. doi: 10.1147/sj.52.0078.
- [2] Rogerio Bonatti, Dan Zhao, Francesco Bonacci, Dillon Dupont, Sara Abdali, Yinheng Li, Yadong Lu, Justin Wagle, Kazuhito Koishida, Arthur Buckner, Lawrence Jang, and Zack Hui. Windows agent arena: Evaluating multi-modal os agents at scale, 2024. URL <https://arxiv.org/abs/2409.08264>.
- [3] Shiyi Cao, Dacheng Li, Fangzhou Zhao, Shuo Yuan, Sumanth R Hegde, Connor Chen, Charlie Ruan, Tyler Griggs, Shu Liu, Eric Tang, et al. Skyrl-agent: Efficient rl training for multi-turn llm agent. *arXiv preprint arXiv:2511.16108*, 2025.
- [4] Ziru Chen, Shijie Chen, Yuting Ning, Qianheng Zhang, Boshi Wang, Botao Yu, Yifei Li, Zeyi Liao, Chen Wei, Zitong Lu, Vishal Dey, Mingyi Xue, Frazier N. Baker, Benjamin Burns, Daniel Adu-Ampratwum, Xuhui Huang, Xia Ning, Song Gao, Yu Su, and Huan Sun. Scienceagentbench: Toward rigorous assessment of language agents for data-driven scientific discovery, 2024. URL <https://arxiv.org/abs/2410.05080>.
- [5] Wei Fu, Jiaxuan Gao, Xujie Shen, Chen Zhu, Zhiyu Mei, Chuyi He, Shusheng Xu, Guo Wei, Jun Mei, Jiashu Wang, Tongkai Yang, Binhang Yuan, and Yi Wu. Areal: A large-scale asynchronous reinforcement learning system for language reasoning, 2025. URL <https://arxiv.org/abs/2505.24298>.
- [6] Wei Gao, Yuheng Zhao, Tianyuan Wu, Shaopan Xiong, Weixun Wang, Dakai An, Lunxi Cao, Dilxat Muhtar, Zichen Liu, Haizhou Zhao, et al. Rollart: Scaling agentic rl training via disaggregated infrastructure. *arXiv preprint arXiv:2512.22560*, 2025.
- [7] Yiyuan He, Minxian Xu, Jingfeng Wu, Jianmin Hu, Chong Ma, Min Shen, Le Chen, Chengzhong Xu, Lin Qu, and Kejiang Ye. Banaserve: Unified kv cache and dynamic module migration for balancing disaggregated llm serving in ai infrastructure, 2025. URL <https://arxiv.org/abs/2510.13223>.
- [8] Naman Jain, King Han, Alex Gu, Wen-Ding Li, Fanjia Yan, Tianjun Zhang, Sida Wang, Armando Solar-Lezama, Koushik Sen, and Ion Stoica. Livecodebench: Holistic and contamination free evaluation of large language models for code, 2024. URL <https://arxiv.org/abs/2403.07974>.
- [9] Dongfu Jiang, Yi Lu, Zhuofeng Li, Zhiheng Lyu, Ping Nie, Haozhe Wang, Alex Su, Hui Chen, Kai Zou, Chao Du, et al. Verltool: Towards holistic agentic reinforcement learning with tool use. *arXiv preprint arXiv:2509.01055*, 2025.
- [10] Carlos E. Jimenez, John Yang, Alexander Wettig, Shunyu Yao, Kexin Pei, Ofir Press, and Karthik Narasimhan. Swe-bench: Can language models resolve real-world github issues?, 2024. URL <https://arxiv.org/abs/2310.06770>.
- [11] Woosuk Kwon, Zhuohan Li, Siyuan Zhuang, Ying Sheng, Lianmin Zheng, Cody Hao Yu, Joseph E. Gonzalez, Hao Zhang, and Ion Stoica. Efficient memory management for large language model serving with pagedattention, 2023. URL <https://arxiv.org/abs/2309.06180>.
- [12] Hanchen Li, Qiuyang Mang, Runyuan He, Qizheng Zhang, Huanzhi Mao, Xiaokun Chen, Hangrui Zhou, Alvin Cheung, Joseph Gonzalez, and Ion Stoica. Continuum: Efficient and robust multi-turn llm agent scheduling with kv cache time-to-live, 2025. URL <https://arxiv.org/abs/2511.02230>.
- [13] Yuhan Liu, Yihua Cheng, Jiayi Yao, Yuwei An, Xiaokun Chen, Shaoting Feng, Yuyang Huang, Samuel Shen, Rui Zhang, Kuntai Du, and Junchen Jiang. Lmcache: An efficient kv cache layer for enterprise-scale llm inference, 2025. URL <https://arxiv.org/abs/2510.09665>.
- [14] Michael Luo, Xiaoxiang Shi, Colin Cai, Tianjun Zhang, Justin Wong, Yichuan Wang, Chi Wang, Yanping Huang, Zhifeng Chen, Joseph E. Gonzalez, and Ion Stoica. Autellix: An efficient serving engine for llm agents as general programs, 2025. URL <https://arxiv.org/abs/2502.13965>.
- [15] Emanuel Parzen. *Stochastic processes*. SIAM, 1999.

- [16] Long Phan, Alice Gatti, Ziwen Han, Nathaniel Li, Josephina Hu, Hugh Zhang, Chen Bo Calvin Zhang, Mohamed Shaaban, John Ling, Sean Shi, Michael Choi, Anish Agrawal, Arnav Chopra, Adam Khoja, Ryan Kim, Richard Ren, Jason Hausenloy, Oliver Zhang, Mantas Mazeika, Dmitry Dodonov, Tung Nguyen, Jaeho Lee, Daron Anderson, Mikhail Doroshenko, Alun Cennyth Stokes, Mobeen Mahmood, Oleksandr Pokutnyi, Oleg Iskra, Jessica P. Wang, John-Clark Levin, Mstyslav Kazakov, Fiona Feng, Steven Y. Feng, Haoran Zhao, Michael Yu, Varun Gangal, Chelsea Zou, Zihan Wang, Serguei Popov, Robert Gerbicz, Geoff Galgon, Johannes Schmitt, Will Yeadon, Yongki Lee, Scott Sauers, Alvaro Sanchez, Fabian Giska, Marc Roth, Søren Riis, Saiteja Utpala, Noah Burns, Gashaw M. Goshu, Mohinder Maheshbhai Naiya, Chidozie Agu, Zachary Giboney, Antrell Cheatom, Francesco Fournier-Facio, Sarah-Jane Crowson, Lennart Finke, Zerui Cheng, Jennifer Zampese, Ryan G. Hoerr, Mark Nandor, Hyunwoo Park, Tim Gehringer, Jiaqi Cai, Ben McCarty, Alexis C Garretson, Edwin Taylor, Damien Sileo, Qiuyu Ren, Usman Qazi, Lianghai Li, Jungbae Nam, John B. Wydallis, Pavel Arkhipov, Jack Wei Lun Shi, Aras Bacho, Chris G. Willcocks, Hangrui Cao, Sumeet Motwani, Emily de Oliveira Santos, Johannes Veith, Edward Vendrow, Doru Cojoc, Kengo Zenitani, Joshua Robinson, Longke Tang, Yuqi Li, Joshua Vendrow, Natanael Wildner Fraga, Vladyslav Kuchkin, Andrey Pupasov Maksimov, Pierre Marion, Denis Efremov, Jayson Lynch, Kaiqu Liang, Aleksandar Mikov, Andrew Gritsevskiy, Julien Guillod, Gözdenur Demir, Dakotah Martinez, Ben Pageler, Kevin Zhou, Saeed Soori, Ori Press, Henry Tang, Paolo Rissone, Sean R. Green, Lina Brüssel, Moon Twayana, Aymeric Dieuleveut, Joseph Marvin Imperial, Ameya Prabhu, Jinzhou Yang, Nick Crispino, Arun Rao, Dimitri Zvonkine, Gabriel Loiseau, Mikhail Kalinin, Marco Lukas, Ciprian Manolescu, Nate Stambaugh, Subrata Mishra, Tad Hogg, Carlo Bosio, Brian P Coppola, Julian Salazar, Jaehyeok Jin, Rafael Sayous, Stefan Ivanov, Philippe Schwaller, Shaipranesh Senthilkuma, Andres M Bran, Andres Algaba, Kelsey Van den Houte, Lynn Van Der Sypt, Brecht Verbeken, David Noever, Alexei Kopylov, Benjamin Myklebust, Bikun Li, Lisa Schut, Evgenii Zheltonozhskii, Qiaochu Yuan, Derek Lim, Richard Stanley, Tong Yang, John Maar, Julian Wykowski, Martí Oller, Anmol Sahu, Cesare Giulio Ardito, Yuzheng Hu, Ariel Ghislain Kemogne Kamdoun, Alvin Jin, Tobias Garcia Vilchis, Yuexuan Zu, Martin Lackner, James Koppel, Gongbo Sun, Daniil S. Antonenko, Steffi Chern, Bingchen Zhao, Pierrot Arsene, Joseph M Cavanagh, Daofeng Li, Jiawei Shen, Donato Crisostomi, Wenjin Zhang, Ali Dehghan, Sergey Ivanov, David Perrella, Nurdin Kaparov, Allen Zang, Ilia Sucholutsky, Arina Kharlamova, Daniil Orel, Vladislav Poritski, Shalev Ben-David, Zachary Berger, Parker Whitfill, Michael Foster, Daniel Munro, Linh Ho, Shankar Sivarajan, Dan Bar Hava, Aleksey Kuchkin, David Holmes, Alexandra Rodriguez-Romero, Frank Sommerhage, Anji Zhang, Richard Moat, Keith Schneider, Zakayo Kazibwe, Don Clarke, Dae Hyun Kim, Felipe Meneguitti Dias, Sara Fish, Veit Elser, Tobias Kreiman, Victor Efren Guadarrama Vilchis, Immo Klose, Ujjwala Anantheswaran, Adam Zweiger, Kaivalya Rawal, Jeffery Li, Jeremy Nguyen, Nicolas Daans, Haline Heidinger, Maksim Radionov, Václav Rozhoň, Vincent Ginis, Christian Stump, Niv Cohen, Rafał Poświata, Josef Tkadlec, Alan Goldfarb, Chenguang Wang, Piotr Padlewski, Stanislaw Barzowski, Kyle Montgomery, Ryan Stendall, Jamie Tucker-Foltz, Jack Stade, T. Ryan Rogers, Tom Goertzen, Declan Grabb, Abhishek Shukla, Alan Givré, John Arnold Ambay, Archan Sen, Muhammad Fayez Aziz, Mark H Inlow, Hao He, Ling Zhang, Younesse Kaddar, Ivar Ångquist, Yanxu Chen, Harrison K Wang, Kalyan Ramakrishnan, Elliott Thornley, Antonio Terpin, Hailey Schoelkopf, Eric Zheng, Avishy Carmi, Ethan D. L. Brown, Kelin Zhu, Max Bartolo, Richard Wheeler, Martin Stehberger, Peter Bradshaw, JP Heimonen, Kaustubh Sridhar, Ido Akov, Jennifer Sandlin, Yury Makarychev, Joanna Tam, Hieu Hoang, David M. Cunningham, Vladimir Goryachev, Demosthenes Patramanis, Michael Krause, Andrew Redenti, David Aldous, Jesyin Lai, Shannon Coleman, Jiangnan Xu, Sangwon Lee, Ilias Magoulas, Sandy Zhao, Ning Tang, Michael K. Cohen, Orr Paradise, Jan Hendrik Kirchner, Maksym Ovchynnikov, Jason O. Matos, Adithya Shenoy, Michael Wang, Yuzhou Nie, Anna Szyber-Betley, Paolo Faraboschi, Robin Riblet, Jonathan Crozier, Shiv Halasyamani, Shreyas Verma, Prashant Joshi, Eli Meril, Ziqiao Ma, Jérémy Andréoletti, Raghav Singhal, Jacob Platnick, Volodymyr Nevirkovets, Luke Basler, Alexander Ivanov, Seri Khoury, Nils Gustafsson, Marco Piccardo, Hamid Mostaghimi, Qijia Chen, Virendra Singh, Tran Quoc Khánh, Paul Rosu, Hannah Szlyk, Zachary Brown, Himanshu Narayan, Aline Menezes, Jonathan Roberts, William Alley, Kunyang Sun, Arkil Patel, Max Lamparth, Anka Reuel, Linwei Xin, Hanmeng Xu, Jacob Loader, Freddie Martin, Zixuan Wang, Andrea Achilleos, Thomas Preu, Tomek Korbak, Ida Bosio, Fereshteh Kazemi, Ziyi Chen, Biró Bálint, Eve J. Y. Lo, Jiaqi Wang, Maria Inês S. Nunes, Jeremiah Milbauer, M Saiful Bari, Zihao Wang, Behzad Ansarinejad, Yewen Sun,

Stephane Durand, Hossam Elgnainy, Guillaume Douville, Daniel Tordera, George Balabanian, Hew Wolff, Lynna Kvistad, Hsiaoyn Milliron, Ahmad Sakor, Murat Eron, Andrew Favre D. O., Shailesh Shah, Xiaoxiang Zhou, Firuz Kamalov, Sherwin Abdoli, Tim Santens, Shaul Barkan, Allison Tee, Robin Zhang, Alessandro Tomasiello, G. Bruno De Luca, Shi-Zhuo Looi, Vinh-Kha Le, Noam Kolt, Jiayi Pan, Emma Rodman, Jacob Drori, Carl J Fossum, Niklas Muennighoff, Milind Jagota, Ronak Pradeep, Honglu Fan, Jonathan Eicher, Michael Chen, Kushal Thaman, William Merrill, Moritz Firsching, Carter Harris, Stefan Ciobăcă, Jason Gross, Rohan Pandey, Ilya Gusev, Adam Jones, Shashank Agnihotri, Pavel Zhelnov, Mohammadreza Mofayez, Alexander Piperski, David K. Zhang, Kostiantyn Dobarskyi, Roman Leventov, Ignat Soroko, Joshua Duersch, Vage Taamazyan, Andrew Ho, Wenjie Ma, William Held, Ruicheng Xian, Armel Randy Zebaze, Mohamad Mohamed, Julian Noah Leser, Michelle X Yuan, Laila Yacar, Johannes Lengler, Katarzyna Olszewska, Claudio Di Fratta, Edson Oliveira, Joseph W. Jackson, Andy Zou, Muthu Chidambaram, Timothy Manik, Hector Haffenden, Dashiell Stander, Ali Dasouqi, Alexander Shen, Bitá Golshani, David Stap, Egor Kretov, Mikalai Uzhou, Alina Borisovna Zhidkovskaya, Nick Winter, Miguel Orbegoza Rodriguez, Robert Lauff, Dustin Wehr, Colin Tang, Zaki Hossain, Shaun Phillips, Fortuna Samuele, Fredrik Ekström, Angela Hammon, Oam Patel, Faraz Farhidi, George Medley, Forough Mohammadzadeh, Madellene Peñaflor, Haile Kassahun, Alena Friedrich, Rayner Hernandez Perez, Daniel Pyda, Taom Sakal, Omkar Dhamane, Ali Khajegili Mirabadi, Eric Hallman, Kenchi Okutsu, Mike Battaglia, Mohammad Maghsoudimehrabani, Alon Amit, Dave Hulbert, Roberto Pereira, Simon Weber, Handoko, Anton Peristy, Stephen Malina, Mustafa Mehkary, Rami Aly, Frank Reidegeld, Anna-Katharina Dick, Cary Friday, Mukhwinder Singh, Hassan Shapourian, Wanyoung Kim, Mariana Costa, Hubeyb Gurdogan, Harsh Kumar, Chiara Ceconello, Chao Zhuang, Haon Park, Micah Carroll, Andrew R. Tawfeek, Stefan Steinerberger, Daattavya Aggarwal, Michael Kirchhof, Linjie Dai, Evan Kim, Johan Ferret, Jainam Shah, Yuzhou Wang, Minghao Yan, Krzysztof Burdzy, Lixin Zhang, Antonio Franca, Diana T. Pham, Kang Yong Loh, Joshua Robinson, Abram Jackson, Paolo Giordano, Philipp Petersen, Adrian Cosma, Jesus Colino, Colin White, Jacob Votava, Vladimir Vinnikov, Ethan Delaney, Petr Spelda, Vit Stritecky, Syed M. Shahid, Jean-Christophe Mourrat, Lavr Vetoshkin, Koen Sponselee, Renas Bacho, Zheng-Xin Yong, Florencia de la Rosa, Nathan Cho, Xiuyu Li, Guillaume Malod, Orion Weller, Guglielmo Albani, Leon Lang, Julien Laurendeau, Dmitry Kazakov, Fatimah Adesanya, Julien Portier, Lawrence Hollom, Victor Souza, Yuchen Anna Zhou, Julien Degorre, Yiğit Yalın, Gbenga Daniel Obikoya, Rai, Filippo Bigi, M. C. Boscá, Oleg Shumar, Kaniuar Bacho, Gabriel Recchia, Mara Popescu, Nikita Shulga, Ngefor Mildred Tanwie, Thomas C. H. Lux, Ben Rank, Colin Ni, Matthew Brooks, Alesia Yakimchyk, Huanxu, Liu, Stefano Cavalleri, Olle Häggström, Emil Verkama, Joshua Newbould, Hans Gundlach, Leonor Brito-Santana, Brian Amaro, Vivek Vajipey, Rynaa Grover, Ting Wang, Yosi Kratish, Wen-Ding Li, Sivakanth Gopi, Andrea Caciolai, Christian Schroeder de Witt, Pablo Hernández-Cámara, Emanuele Rodolà, Jules Robins, Dominic Williamson, Vincent Cheng, Brad Raynor, Hao Qi, Ben Segev, Jingxuan Fan, Sarah Martinson, Erik Y. Wang, Kaylie Hausknecht, Michael P. Brenner, Mao Mao, Christoph Demian, Peyman Kassani, Xinyu Zhang, David Avagian, Eshawn Jessica Scipio, Alon Ragoler, Justin Tan, Blake Sims, Rebeka Plecnik, Aaron Kirtland, Omer Faruk Bodur, D. P. Shinde, Yan Carlos Leyva Labrador, Zahra Adoul, Mohamed Zekry, Ali Karakoc, Tania C. B. Santos, Samir Shamseldeen, Loukmane Karim, Anna Liakhovitskaia, Nate Resman, Nicholas Farina, Juan Carlos Gonzalez, Gabe Maayan, Earth Anderson, Rodrigo De Oliveira Pena, Elizabeth Kelley, Hodjat Mariji, Rasoul Pouriamanesh, Wentao Wu, Ross Finocchio, Ismail Alarab, Joshua Cole, Danyelle Ferreira, Bryan Johnson, Mohammad Safdari, Liangti Dai, Siriphan Arthornthurasuk, Isaac C. McAlister, Alejandro José Moyano, Alexey Pronin, Jing Fan, Angel Ramirez-Trinidad, Yana Malysheva, Daphiny Pottmaier, Omid Taheri, Stanley Stepanic, Samuel Perry, Luke Askew, Raúl Adrián Huerta Rodríguez, Ali M. R. Minissi, Ricardo Lorena, Krishnamurthy Iyer, Arshad Anil Fasiludeen, Ronald Clark, Josh Ducey, Matheus Piza, Maja Somrak, Eric Vergo, Juehang Qin, Benjámín Borbás, Eric Chu, Jack Lindsey, Antoine Jallon, I. M. J. McInnis, Evan Chen, Avi Semler, Luk Gloor, Tej Shah, Marc Carauleanu, Pascal Lauer, Tran Duc Huy, Hossein Shahrtash, Emilien Duc, Lukas Lewark, Assaf Brown, Samuel Albanie, Brian Weber, Warren S. Vaz, Pierre Clavier, Yiyang Fan, Gabriel Poesia Reis e Silva, Long, Lian, Marcus Abramovitch, Xi Jiang, Sandra Mendoza, Murat Islam, Juan Gonzalez, Vasiliios Mavroudis, Justin Xu, Pawan Kumar, Laxman Prasad Goswami, Daniel Bugas, Nasser Heydari, Ferenc Jeanplong, Thorben Jansen, Antonella Pinto, Archimedes Apronti, Abdallah Galal, Ng Ze-An, Ankit Singh, Tong Jiang, Joan of Arc Xavier, Kanu Priya Agarwal, Mohammed Berkani, Gang Zhang, Zhehang Du,

Benedito Alves de Oliveira Junior, Dmitry Malishev, Nicolas Remy, Taylor D. Hartman, Tim Tarver, Stephen Mensah, Gautier Abou Loume, Wiktor Morak, Farzad Habibi, Sarah Hoback, Will Cai, Javier Gimenez, Roselynn Grace Montecillo, Jakub Lucki, Russell Campbell, Asankhaya Sharma, Khalida Meer, Shreen Gul, Daniel Espinosa Gonzalez, Xavier Alapont, Alex Hoover, Gunjan Chhablani, Freddie Vargus, Arunim Agarwal, Yibo Jiang, Deepakkumar Patil, David Outevsky, Kevin Joseph Scaria, Rajat Maheshwari, Abdelkader Dendane, Priti Shukla, Ashley Cartwright, Sergei Bogdanov, Niels Mündler, Sören Möller, Luca Arnaboldi, Kunvar Thaman, Muhammad Rehan Siddiqi, Prajvi Saxena, Himanshu Gupta, Tony Fruhauff, Glen Sherman, Mátyás Vincze, Siranut Usawasutsakorn, Dylan Ler, Anil Radhakrishnan, Innocent Enyekwe, Sk Md Salaudhin, Jiang Muzhen, Aleksandr Maksapetyan, Vivien Rossbach, Chris Harjadi, Mohsen Bahalooohoreh, Claire Sparrow, Jasdeep Sidhu, Sam Ali, Song Bian, John Lai, Eric Singer, Justine Leon Uro, Greg Bateman, Mohamed Sayed, Ahmed Menshawy, Darling Duclosel, Dario Bezzi, Yashaswini Jain, Ashley Aaron, Murat Tiryakioglu, Sheeshram Siddh, Keith Krenek, Imad Ali Shah, Jun Jin, Scott Creighton, Denis Peskoff, Zienab EL-Wasif, Ragavendran P V, Michael Richmond, Joseph McGowan, Tejal Patwardhan, Hao-Yu Sun, Ting Sun, Nikola Zubić, Samuele Sala, Stephen Ebert, Jean Kaddour, Manuel Schottdorf, Dianzhuo Wang, Gerol Petruzella, Alex Meiburg, Tilen Medved, Ali ElSheikh, S Ashwin Hebbar, Lorenzo Vaquero, Xianjun Yang, Jason Poulos, Vilém Zouhar, Sergey Bogdanik, Mingfang Zhang, Jorge Sanz-Ros, David Anugraha, Yinwei Dai, Anh N. Nhu, Xue Wang, Ali Anil Demircali, Zhibai Jia, Yuyin Zhou, Juncheng Wu, Mike He, Nitin Chandok, Aarush Sinha, Gaoxiang Luo, Long Le, Mickaël Noyé, Michał Perelkiewicz, Ioannis Pantidis, Tianbo Qi, Soham Sachin Purohit, Letitia Parcalabescu, Thai-Hoa Nguyen, Genta Indra Winata, Edoardo M. Ponti, Hanchen Li, Kaustubh Dhole, Jongee Park, Dario Abbondanza, Yuanli Wang, Anupam Nayak, Diogo M. Caetano, Antonio A. W. L. Wong, Maria del Rio-Chanona, Dániel Kondor, Pieter Francois, Ed Chalstrey, Jakob Zsambok, Dan Hoyer, Jenny Reddish, Jakob Hauser, Francisco-Javier Rodrigo-Ginés, Suchandra Datta, Maxwell Shepherd, Thom Kamphuis, Qizheng Zhang, Hyunjun Kim, Ruiji Sun, Jianzhu Yao, Franck Dernoncourt, Satyapriya Krishna, Sina Rismanchian, Bonan Pu, Francesco Pinto, Yingheng Wang, Kumar Shridhar, Kalon J. Overholt, Glib Briia, Hieu Nguyen, David, Soler Bartomeu, Tony CY Pang, Adam Wecker, Yifan Xiong, Fanfei Li, Lukas S. Huber, Joshua Jaeger, Romano De Maddalena, Xing Han Lù, Yuhui Zhang, Claas Beger, Patrick Tser Jern Kon, Sean Li, Vivek Sanker, Ming Yin, Yihao Liang, Xinlu Zhang, Ankit Agrawal, Li S. Yifei, Zechen Zhang, Mu Cai, Yasin Sonmez, Costin Cozianu, Changhao Li, Alex Slen, Shoubin Yu, Hyun Kyu Park, Gabriele Sarti, Marcin Briański, Alessandro Stolfo, Truong An Nguyen, Mike Zhang, Yotam Perlit, Jose Hernandez-Orallo, Runjia Li, Amin Shabani, Felix Juefei-Xu, Shikhar Dhingra, Orr Zohar, My Chiffon Nguyen, Alexander Pondaven, Abdurrahim Yilmaz, Xuandong Zhao, Chuanyang Jin, Muyan Jiang, Stefan Todoran, Xinyao Han, Jules Kreuer, Brian Rabern, Anna Plassart, Martino Maggetti, Luther Yap, Robert Geirhos, Jonathon Kean, Dingsu Wang, Sina Mollaei, Chenkai Sun, Yifan Yin, Shiqi Wang, Rui Li, Yaowen Chang, Anjiang Wei, Alice Bizeul, Xiaohan Wang, Alexandre Oliveira Arrais, Kushin Mukherjee, Jorge Chamorro-Padial, Jiachen Liu, Xingyu Qu, Junyi Guan, Adam Bouyamourn, Shuyu Wu, Martyna Plomecka, Junda Chen, Mengze Tang, Jiaqi Deng, Shreyas Subramanian, Haocheng Xi, Haoxuan Chen, Weizhi Zhang, Yinuo Ren, Haoqin Tu, Sejong Kim, Yushun Chen, Sara Vera Marjanović, Junwoo Ha, Grzegorz Luczyna, Jeff J. Ma, Zewen Shen, Dawn Song, Cedegao E. Zhang, Zhun Wang, Gaël Gendron, Yunze Xiao, Leo Smucker, Erica Weng, Kwok Hao Lee, Zhe Ye, Stefano Ermon, Ignacio D. Lopez-Miguel, Theo Knights, Anthony Gitter, Namkyu Park, Boyi Wei, Hongzheng Chen, Kunal Pai, Ahmed Elkhanany, Han Lin, Philipp D. Siedler, Jichao Fang, Ritwik Mishra, Károly Zsolnai-Fehér, Xilin Jiang, Shadab Khan, Jun Yuan, Rishab Kumar Jain, Xi Lin, Mike Peterson, Zhe Wang, Aditya Malusare, Maosen Tang, Isha Gupta, Ivan Fosin, Timothy Kang, Barbara Dworakowska, Kazuki Matsumoto, Guangyao Zheng, Gerben Sewuster, Jorge Pretel Villanueva, Ivan Rannev, Igor Chernyavsky, Jiale Chen, Deepayan Banik, Ben Racz, Wenchao Dong, Jianxin Wang, Laila Bashmal, Duarte V. Gonçalves, Wei Hu, Kaushik Bar, Ondrej Bohdal, Atharv Singh Patlan, Shehzaad Dhuliawala, Caroline Geirhos, Julien Wist, Yuval Kansal, Bingsen Chen, Kutay Tire, Atak Talay Yücel, Brandon Christof, Veerupaksh Singla, Zijian Song, Sanxing Chen, Jiaxin Ge, Kaustubh Ponskshe, Isaac Park, Tianneng Shi, Martin Q. Ma, Joshua Mak, Sherwin Lai, Antoine Moulin, Zhuo Cheng, Zhanda Zhu, Ziyi Zhang, Vaidehi Patil, Ketan Jha, Qiutong Men, Jiaxuan Wu, Tianchi Zhang, Bruno Hebling Vieira, Alham Fikri Aji, Jae-Won Chung, Mohammed Mahfoud, Ha Thi Hoang, Marc Sperzel, Wei Hao, Kristof Meding, Sihan Xu, Vassilis Kostakos, Davide Manini, Yueying Liu, Christopher Toukmaji, Jay Paek, Eunmi Yu, Arif Engin Demircali, Zhiyi Sun, Ivan Dewerpe, Hongsen Qin, Roman Pflugfelder,

James Bailey, Johnathan Morris, Ville Heilala, Sybille Rosset, Zishun Yu, Peter E. Chen, Woongyeong Yeo, Eeshaan Jain, Ryan Yang, Sreekar Chigurupati, Julia Chernyavsky, Sai Prajwal Reddy, Subhashini Venugopalan, Hunar Batra, Core Francisco Park, Hieu Tran, Guilherme Maximiano, Genghan Zhang, Yizhuo Liang, Hu Shiyu, Rongwu Xu, Rui Pan, Siddharth Suresh, Ziqi Liu, Samaksh Gulati, Songyang Zhang, Peter Turchin, Christopher W. Bartlett, Christopher R. Scotese, Phuong M. Cao, Ben Wu, Jacek Karwowski, Davide Scaramuzza, Aakaash Nattanmai, Gordon McKellips, Anish Cheraku, Asim Suhail, Ethan Luo, Marvin Deng, Jason Luo, Ashley Zhang, Kavin Jindel, Jay Paek, Kasper Halevy, Allen Baranov, Michael Liu, Advait Avadhanam, David Zhang, Vincent Cheng, Brad Ma, Evan Fu, Liam Do, Joshua Lass, Hubert Yang, Surya Sunkari, Vishruth Bharath, Violet Ai, James Leung, Rishit Agrawal, Alan Zhou, Kevin Chen, Tejas Kalpathi, Ziqi Xu, Gavin Wang, Tyler Xiao, Erik Maung, Sam Lee, Ryan Yang, Roy Yue, Ben Zhao, Julia Yoon, Sunny Sun, Aryan Singh, Ethan Luo, Clark Peng, Tyler Osbey, Taozhi Wang, Daryl Echeazu, Hubert Yang, Timothy Wu, Spandan Patel, Vidhi Kulkarni, Vijaykaarti Sundarapandiyan, Ashley Zhang, Andrew Le, Zafir Nasim, Srikar Yalam, Ritesh Kasamsetty, Soham Samal, Hubert Yang, David Sun, Nihar Shah, Abhijeet Saha, Alex Zhang, Leon Nguyen, Laasya Nagumalli, Kaixin Wang, Alan Zhou, Aidan Wu, Jason Luo, Anwith Telluri, Summer Yue, Alexandr Wang, and Dan Hendrycks. Humanity’s last exam, 2025. URL <https://arxiv.org/abs/2501.14249>.

- [17] Idan Shenfeld, Jyothish Pari, and Pulkit Agrawal. RL’s razor: Why online reinforcement learning forgets less, 2025. URL <https://arxiv.org/abs/2509.04259>.
- [18] Guangming Sheng, Chi Zhang, Zilingfeng Ye, Xibin Wu, Wang Zhang, Ru Zhang, Yanghua Peng, Haibin Lin, and Chuan Wu. Hybridflow: A flexible and efficient rlhf framework. In *Proceedings of the Twentieth European Conference on Computer Systems*, EuroSys ’25, pp. 1279–1297. ACM, March 2025. doi: 10.1145/3689031.3696075. URL <http://dx.doi.org/10.1145/3689031.3696075>.
- [19] Hongjin Su, Shizhe Diao, Ximing Lu, Mingjie Liu, Jiacheng Xu, Xin Dong, Yonggan Fu, Peter Belcak, Hanrong Ye, Hongxu Yin, Yi Dong, Evelina Bakhturina, Tao Yu, Yejin Choi, Jan Kautz, and Pavlo Molchanov. Toolorchestra: Elevating intelligence via efficient model and tool orchestration, 2025. URL <https://arxiv.org/abs/2511.21689>.
- [20] Hanshi Sun, Li-Wen Chang, Wenlei Bao, Size Zheng, Ningxin Zheng, Xin Liu, Harry Dong, Yuejie Chi, and Beidi Chen. Shadowkv: Kv cache in shadows for high-throughput long-context llm inference, 2025. URL <https://arxiv.org/abs/2410.21465>.
- [21] 5 Team, Aohan Zeng, Xin Lv, Qinkai Zheng, Zhenyu Hou, Bin Chen, Chengxing Xie, Cunxiang Wang, Da Yin, Hao Zeng, Jiajie Zhang, Kedong Wang, Lucen Zhong, Mingdao Liu, Rui Lu, Shulin Cao, Xiaohan Zhang, Xuancheng Huang, Yao Wei, Yean Cheng, Yifan An, Yilin Niu, Yuanhao Wen, Yushi Bai, Zhengxiao Du, Zihan Wang, Zilin Zhu, Bohan Zhang, Bosi Wen, Bowen Wu, Bowen Xu, Can Huang, Casey Zhao, Changpeng Cai, Chao Yu, Chen Li, Chendi Ge, Chenghua Huang, Chenhui Zhang, Chenxi Xu, Chenzheng Zhu, Chuang Li, Congfeng Yin, Daoyan Lin, Dayong Yang, Dazhi Jiang, Ding Ai, Erle Zhu, Fei Wang, Gengzheng Pan, Guo Wang, Hailong Sun, Haitao Li, Haiyang Li, Haiyi Hu, Hanyu Zhang, Hao Peng, Hao Tai, Haoke Zhang, Haoran Wang, Haoyu Yang, He Liu, He Zhao, Hongwei Liu, Hongxi Yan, Huan Liu, Huilong Chen, Ji Li, Jiajing Zhao, Jiamin Ren, Jian Jiao, Jiani Zhao, Jianyang Yan, Jiaqi Wang, Jiayi Gui, Jiayue Zhao, Jie Liu, Jijie Li, Jing Li, Jing Lu, Jingsen Wang, Jingwei Yuan, Jingxuan Li, Jingzhao Du, Jinhua Du, Jinxin Liu, Junkai Zhi, Junli Gao, Ke Wang, Lekang Yang, Liang Xu, Lin Fan, Lindong Wu, Lintao Ding, Lu Wang, Man Zhang, Minghao Li, Minghuan Xu, Mingming Zhao, Mingshu Zhai, Pengfan Du, Qian Dong, Shangde Lei, Shangqing Tu, Shangtong Yang, Shaoyou Lu, Shijie Li, Shuang Li, Shuang-Li, Shuxun Yang, Siboyi, Tianshu Yu, Wei Tian, Weihang Wang, Wenbo Yu, Weng Lam Tam, Wenjie Liang, Wentao Liu, Xiao Wang, Xiaohan Jia, Xiaotao Gu, Xiaoying Ling, Xin Wang, Xing Fan, Xingru Pan, Xinyuan Zhang, Xinze Zhang, Xiuqing Fu, Xunkai Zhang, Yabo Xu, Yandong Wu, Yida Lu, Yidong Wang, Yilin Zhou, Yiming Pan, Ying Zhang, Yingli Wang, Yingru Li, Yinpei Su, Yipeng Geng, Yitong Zhu, Yongkun Yang, Yuhang Li, Yuhao Wu, Yujiang Li, Yunan Liu, Yunqing Wang, Yuntao Li, Yuxuan Zhang, Zezhen Liu, Zhen Yang, Zhengda Zhou, Zhongpei Qiao, Zhuoer Feng, Zhuorui Liu, Zichen Zhang, Zihan Wang, Zijun Yao, Zikang Wang, Ziqiang Liu, Ziwei Chai, Zixuan Li, Zuodong Zhao, Wenguang Chen, Jidong Zhai, Bin Xu, Minlie Huang, Hongning Wang,

- Juanzi Li, Yuxiao Dong, and Jie Tang. Glm-4.5: Agentic, reasoning, and coding (arc) foundation models, 2025. URL <https://arxiv.org/abs/2508.06471>.
- [22] vLLM Team. KV-aware Routing — vLLM Production Stack Documentation. <https://docs.vllm.ai/projects/production-stack/en/vllm-stack-0.1.5/tutorials/kvaware.html>, 2025. Accessed: 2026-01-15.
- [23] Weixun Wang, XiaoXiao Xu, Wanhe An, Fangwen Dai, Wei Gao, Yancheng He, Ju Huang, Qiang Ji, Hanqi Jin, Xiaoyang Li, et al. Let it flow: Agentic crafting on rock and roll, building the rome model within an open agentic learning ecosystem. *arXiv preprint arXiv:2512.24873*, 2025.
- [24] Xingyao Wang, Boxuan Li, Yufan Song, Frank F. Xu, Xiangru Tang, Mingchen Zhuge, Jiayi Pan, Yueqi Song, Bowen Li, Jaskirat Singh, Hoang H. Tran, Fuqiang Li, Ren Ma, Mingzhang Zheng, Bill Qian, Yanjun Shao, Niklas Muennighoff, Yizhe Zhang, Binyuan Hui, Junyang Lin, Robert Brennan, Hao Peng, Heng Ji, and Graham Neubig. Openhands: An open platform for ai software developers as generalist agents, 2025. URL <https://arxiv.org/abs/2407.16741>.
- [25] Tianbao Xie, Danyang Zhang, Jixuan Chen, Xiaochuan Li, Siheng Zhao, Ruisheng Cao, Toh Jing Hua, Zhoujun Cheng, Dongchan Shin, Fangyu Lei, Yitao Liu, Yiheng Xu, Shuyan Zhou, Silvio Savarese, Caiming Xiong, Victor Zhong, and Tao Yu. Osvorld: Benchmarking multimodal agents for open-ended tasks in real computer environments, 2024. URL <https://arxiv.org/abs/2404.07972>.
- [26] Zhiqiang Xie, Ziyi Xu, Mark Zhao, Yuwei An, Vikram Sharma Mailthody, Scott Mahlke, Michael Garland, and Christos Kozyrakis. Strata: Hierarchical context caching for long context language model serving, 2025. URL <https://arxiv.org/abs/2508.18572>.
- [27] An Yang, Anfeng Li, Baosong Yang, Beichen Zhang, Binyuan Hui, Bo Zheng, Bowen Yu, Chang Gao, Chengen Huang, Chenxu Lv, Chujie Zheng, Dayiheng Liu, Fan Zhou, Fei Huang, Feng Hu, Hao Ge, Haoran Wei, Huan Lin, Jialong Tang, Jian Yang, Jianhong Tu, Jianwei Zhang, Jianxin Yang, Jiayi Yang, Jing Zhou, Jingren Zhou, Junyang Lin, Kai Dang, Keqin Bao, Kexin Yang, Le Yu, Lianghao Deng, Mei Li, Mingfeng Xue, Mingze Li, Pei Zhang, Peng Wang, Qin Zhu, Rui Men, Ruize Gao, Shixuan Liu, Shuang Luo, Tianhao Li, Tianyi Tang, Wenbiao Yin, Xingzhang Ren, Xinyu Wang, Xinyu Zhang, Xuancheng Ren, Yang Fan, Yang Su, Yichang Zhang, Yinger Zhang, Yu Wan, Yuqiong Liu, Zekun Wang, Zeyu Cui, Zhenru Zhang, Zhipeng Zhou, and Zihan Qiu. Qwen3 technical report, 2025. URL <https://arxiv.org/abs/2505.09388>.
- [28] John Yang, Carlos E. Jimenez, Alexander Wettig, Kilian Lieret, Shunyu Yao, Karthik Narasimhan, and Ofir Press. Swe-agent: Agent-computer interfaces enable automated software engineering, 2024. URL <https://arxiv.org/abs/2405.15793>.
- [29] Lingfan Yu, Jinkun Lin, and Jinyang Li. Stateful large language model serving with pensieve. In *Proceedings of the Twentieth European Conference on Computer Systems*, EuroSys ’25, pp. 144–158. ACM, March 2025. doi: 10.1145/3689031.3696086. URL <http://dx.doi.org/10.1145/3689031.3696086>.
- [30] Yichao Yuan, Advait Iyer, Lin Ma, and Nishil Talati. Vortex: Overcoming memory capacity limitations in gpu-accelerated large-scale data analytics, 2025. URL <https://arxiv.org/abs/2502.09541>.
- [31] Hanchen Zhang, Xiao Liu, Bowen Lv, Xueqiao Sun, Bohao Jing, Iat Long Iong, Zhenyu Hou, Zehan Qi, Hanyu Lai, Yifan Xu, et al. Agentrl: Scaling agentic reinforcement learning with a multi-turn, multi-task framework. *arXiv preprint arXiv:2510.04206*, 2025.
- [32] Lei Zhang, Mouxiang Chen, Ruisheng Cao, Jiawei Chen, Fan Zhou, Yiheng Xu, Jiayi Yang, Liang Chen, Changwei Luo, Kai Zhang, et al. MegafLOW: Large-scale distributed orchestration system for the agentic era. *arXiv preprint arXiv:2601.07526*, 2026.
- [33] Chujie Zheng, Kai Dang, Bowen Yu, Mingze Li, Huiqiang Jiang, Junrong Lin, Yuqiong Liu, Hao Lin, Chencan Wu, Feng Hu, An Yang, Jingren Zhou, and Junyang Lin. Stabilizing reinforcement learning with llms: Formulation and practices, 2025. URL <https://arxiv.org/abs/2512.01374>.

- [34] Lianmin Zheng, Liangsheng Yin, Zhiqiang Xie, Chuyue Sun, Jeff Huang, Cody Hao Yu, Shiyi Cao, Christos Kozyrakis, Ion Stoica, Joseph E. Gonzalez, Clark Barrett, and Ying Sheng. Sglang: Efficient execution of structured language model programs, 2024. URL <https://arxiv.org/abs/2312.07104>.
- [35] Yinmin Zhong, Shengyu Liu, Junda Chen, Jianbo Hu, Yibo Zhu, Xuanzhe Liu, Xin Jin, and Hao Zhang. Distserve: Disaggregating prefill and decoding for goodput-optimized large language model serving, 2024. URL <https://arxiv.org/abs/2401.09670>.
- [36] Shuyan Zhou, Frank F. Xu, Hao Zhu, Xuhui Zhou, Robert Lo, Abishek Sridhar, Xianyi Cheng, Tianyue Ou, Yonatan Bisk, Daniel Fried, Uri Alon, and Graham Neubig. Webarena: A realistic web environment for building autonomous agents, 2024. URL <https://arxiv.org/abs/2307.13854>.

## A Extended Discussion

### A.1 KV Cache Optimization

**Multi-tiered KV cache management.** To alleviate GPU memory pressure, systems such as Pensieve [29], Continuum [12], Strata [26], and ShadowKV [20] exploit the hardware memory hierarchy, comprising GPU HBM, CPU DRAM, and NVMe SSD for KV cache management. These tiered caching mechanisms mitigate transient preemption by offloading inactive KV states to lower-tier storage and prefetching them back to GPU upon request resumption. However, the practical efficiency of these methods is fundamentally constrained by the inter-tier bandwidth between device and host memory. In high-frequency agentic workflows, the overhead of frequent swap-in and swap-out cycles often negates the benefits of multi-tier caching as shown in Section 5.

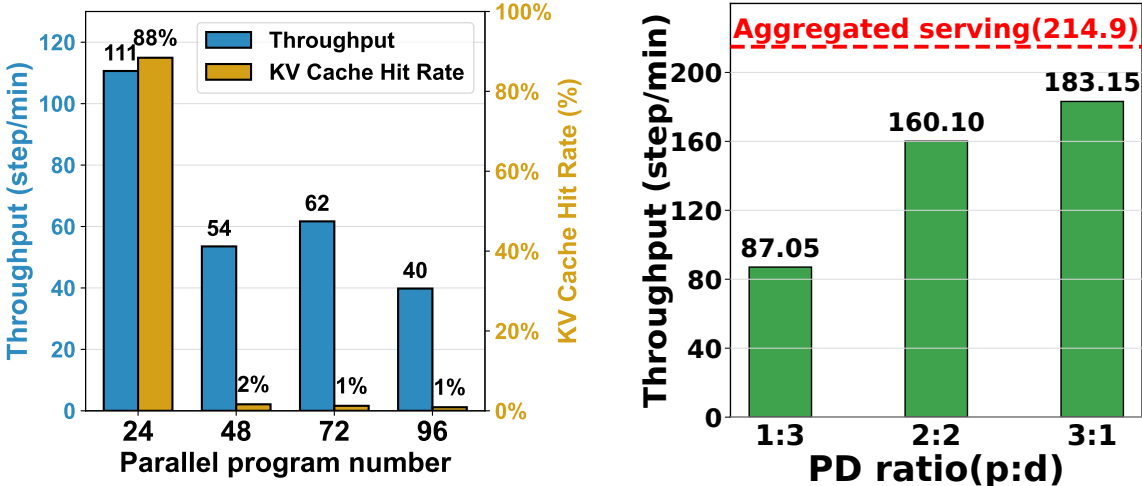
**Distributed KV cache management.** Distributed management of agentic states introduces significant complexity to KV cache eviction and preemption policies. While systems like BanaServe [7] and LMCache [13] enable KV cache transfer across DP nodes, their performance in large-batch agentic serving and rollout is often constrained by limited interconnect bandwidth. The strong intra-program dependencies in agentic workflows necessitate frequent state transferring without program-level management, which can easily saturate the network during serving or rollout.

To bypass these bandwidth bottlenecks, standard inference systems like vLLM KV-aware router [22] and SGLang Model Gateway [34] employ KV-aware routing policies that pin requests to specific nodes based on prefix locality or session ID. Similarly, Vortex [30] introduces session-aware prefetching to minimize cross-node data transfer latency. However, these approaches lack the capability to dynamically migrate active program states between DP nodes. This absence of workload transfer leads to severe memory utilization imbalance across the cluster, shown in Figure 2a. Nodes hosting long-running agentic programs cannot offload states to idle peers, resulting in fragmented resource utilization and degraded aggregate throughput.

### A.2 Existing KV cache optimization methods

**KV cache offloading.** We investigated KV cache offloading by using LMCache [13] as a potential remedy for capacity constraints. While offloading theoretically extends effective memory space by utilizing CPU or SSD storage, our implementation with vLLM + LMCache reveals a critical bottleneck: the PCIe bandwidth is insufficient to sustain the high-frequency context switching and large-volume data transfers inherent to agentic workloads. As demonstrated in Figure 7a, when serving the GLM-4.6 model [21] with the mini-SWEAgent framework [28], the latency penalty from frequent swap-in and swap-out operations negates the memory capacity benefits, resulting in severe throughput degradation under heavy agentic workloads.

**Prefill-Decode (PD) disaggregation.** We also explored PD disaggregation [35], a standard optimization for chatbot serving by isolating the decoding phase from prefill interference. However, when applied to agentic workloads characterized by continuous context growth, we observe that PD disaggregation *exacerbates* thrashing. By partitioning the cluster into prefill-only and decode-only nodes, the effective HBM pool available for handling prefill is significantly smaller than that in a unified architecture. This memory fragmentation causes the system to hit capacity limits and trigger thrashing at much lower concurrency levels, as shown in Figure 7b. These results demonstrate that generic architectural optimizations cannot substitute for a program-centric scheduler that actively manages the working set.



(a) KV Cache Hit Rate with KV Cache Offloading (b) Throughput v.s. Prefill-Only/Decode-Only Node Ratio

Figure 7: Ablation study on KV cache offloading and Prefill-Decode (PD) disaggregation

### A.3 Scaling up agentic workflows

**Heterogeneous resource allocation and scheduling.** To orchestrate multi-turn agent-environment interactions at scale, recent systems such as MegaFlow [32], RollArt [6, 23], AgentRL [31], and VerlTool [9] decouple model inference from environment execution. While these frameworks effectively scale environment concurrency via specialized services, they exhibit the inherent limitations of coarse-grained disaggregation. By treating the inference engine and tool executor as isolated black boxes, these systems lack unified resource management and are unable to coordinate KV cache lifecycles with the environment execution. Without fine-grained scheduling at program-level, disaggregation-based approaches waste KV cache reuse potential in agentic workloads, yielding sub-optimal throughput.

**Scalability of ThunderAgent as a Routing Policy** For multi-node deployment, ThunderAgent replaces session-based static node-pinning with a global waiting queue. When a paused workflow is ready to resume, ThunderAgent routes its requests to the node with the most available capacity. Such routing strategy balances the tradeoff between KV cache locality and multi-node workload balance, achieving both efficient cache utilization and even load distribution across the cluster.

The main paper’s distributed-rollout result (Table 2) uses the standard 2-node setting; we now extend the experiment to up to 8 nodes ( $64 \times H100$ ) on the same GLM-4.6 + mini-SWEAgent workload, with concurrency scaled proportionally (72 programs per node). The baseline is the *Cache-Aware Routing Policy* in SGLang Model Gateway<sup>2</sup>, which pins requests to specific backend replicas based on prefix locality but cannot redistribute paused programs across nodes.

Figure 8 compares throughput against this baseline and against an idealized linear-scaling reference. THUNDERAGENT tracks the linear-scaling line closely from 2 to 8 nodes, whereas the Cache-Aware Routing Policy quickly falls off because cross-node memory imbalance grows with cluster size and a locality-only router cannot rebalance the paused-program pool (cf. Section G.1). Concretely, THUNDERAGENT’s speedup over the SGLang baseline *widens* from  $1.79 \times$  at 2 nodes to  $2.39 \times$  at 8 nodes. We also instrumented the per-tick communication delay of THUNDERAGENT’s global scheduler: it grows sub-linearly from 13.5 ms at 2 nodes to 22.7 ms at 8 nodes (i.e.,  $1.68 \times$  for a  $4 \times$  increase in nodes) and remains well below per-step inference latency, which is on the order of seconds. The global scheduler is therefore not a bottleneck for scaling.

<sup>2</sup>[https://docs.sglang.io/docs/advanced\\_features/sgl\\_model\\_gateway#cache-aware-policy-tuning](https://docs.sglang.io/docs/advanced_features/sgl_model_gateway#cache-aware-policy-tuning)

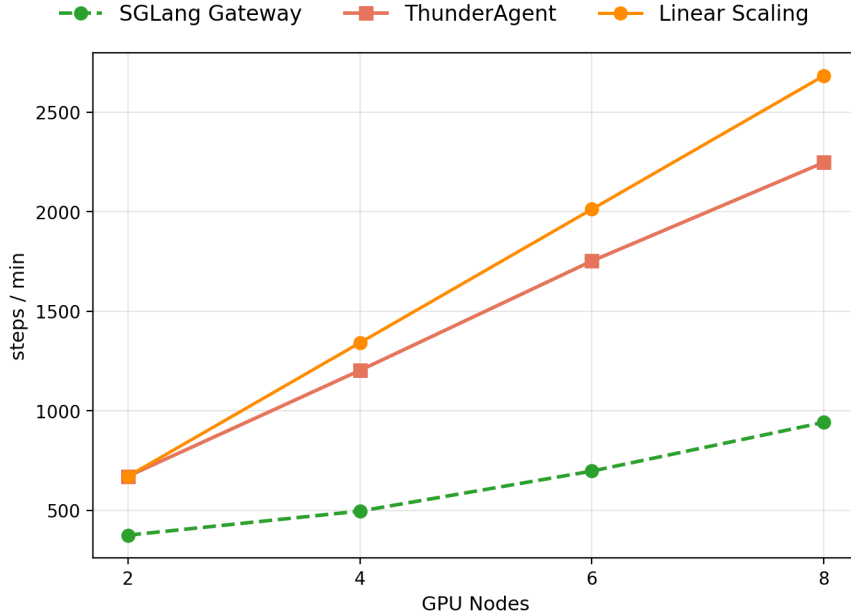


Figure 8: **Scaling up ThunderAgent to 8 H100 nodes**, GLM-4.6 + mini-SWEAgent (72 concurrent programs per node). THUNDERAGENT tracks the ideal linear-scaling reference, while the Cache-Aware Routing Policy in SGLang Model Gateway falls progressively further behind as the cluster grows.

#### A.4 Compatibility of ThunderAgent with KV-cache offloading

THUNDERAGENT is orthogonal to KV-cache offloading and remains effective when offloading is enabled. To demonstrate this, we integrate THUNDERAGENT into **SGLang HiCache** [26] with the host-memory ratio set to 2.0, serving **MiniMax M2.5** on **R2E-Gym** across 8×H100 GPUs. We sweep serving batch size from 64 to 192 and compare against the same SGLang + HiCache stack *without* THUNDERAGENT as the baseline.

**Offloading alone is insufficient at high concurrency.** Figure 9 shows that the baseline keeps a high throughput up to batch size 96, where the combined host + device capacity still accommodates the working set. As we push to batch sizes 160 and 192, however, the baseline’s combined capacity is exhausted: P50 latency jumps from ~10 s to ~30 s at batch 160 and to ~70 s at batch 192, while throughput *decreases* despite the larger batch.

**ThunderAgent prevents capacity collapse and improves throughput at every batch size.** By temporarily pausing short programs to keep the live working set within available capacity, THUNDERAGENT holds both P50 and P90 latency essentially flat at ~10 s and ~20 s respectively across the entire sweep, while throughput grows monotonically with batch size. Even at small batch sizes where both methods achieve high cache hit via PCIe swapping, THUNDERAGENT still improves throughput and latency by selectively pausing acting programs.

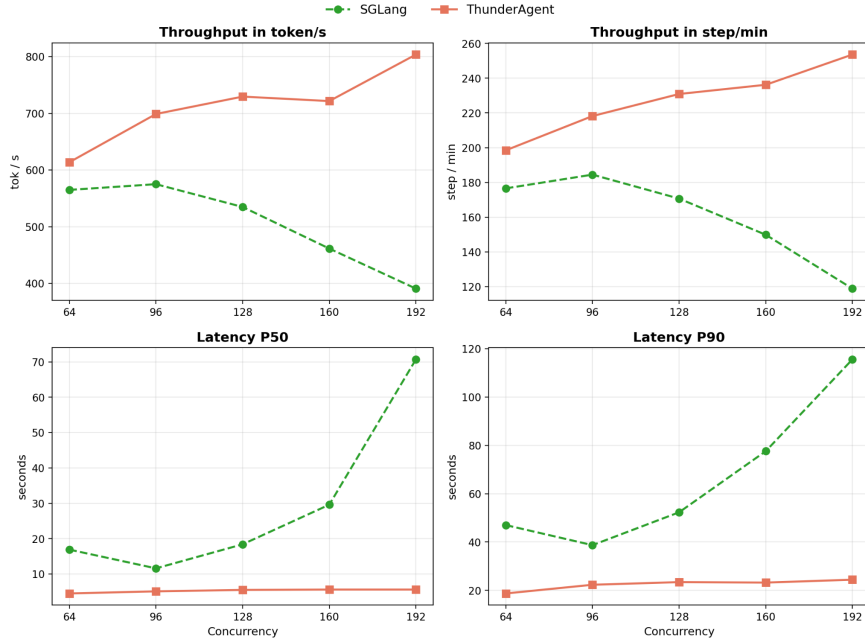


Figure 9: THUNDERAGENT with SGLang HiCache

## A.5 Portability of ThunderAgent across Hardware Generations

We test THUNDERAGENT on hardware with a lower compute-to-bandwidth ratio than H100. Table 3 reports the relevant ratio for the two GPU tiers we use in the paper: the A100 sits at 153 GFLOPS/GB, roughly half H100’s 295.

Figure 10 reports throughput on  $8 \times A100$  with the same workloads as Figure 4(a, b). At low concurrency (24), THUNDERAGENT matches vLLM within noise on both pipelines, because the working set fits comfortably in HBM and thrashing is rare. As concurrency rises to 48 and 72, the picture flips: THUNDERAGENT widens the gap to 1.71–2.08 $\times$  on mini-SWEAgent and 1.16–1.62 $\times$  on OpenHands, while vLLM’s throughput *decreases* from concurrency 48 onward as it begins to thrash.

GPU	Compute (TFLOPs)	Bandwidth (GB/s)	Ratio
H100	989	3350	295.2
A100	312	2039	153.0

Table 3: Compute-to-bandwidth ratio across hardware tiers. We report FP16 Tensor Core (without sparsity) compute performance in TFLOPs and Global-to-L2 memory bandwidth in GB/s.

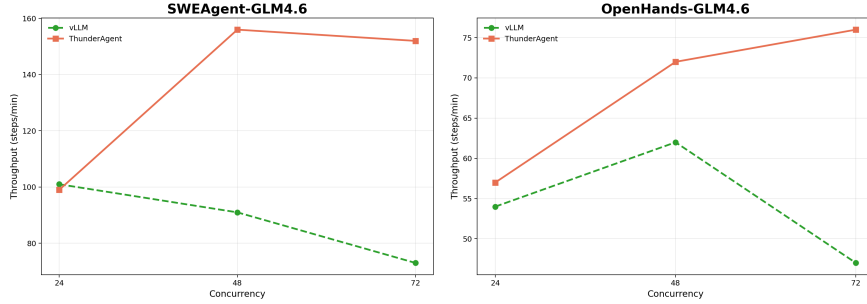


Figure 10: THUNDERAGENT on A100 GPUs

## A.6 Adoption of ThunderAgent in Open-Source Frameworks

Beyond our own evaluation, THUNDERAGENT has been adopted by open-source RL and serving frameworks to accelerate agentic rollout and serving, demonstrating that it can be integrated into existing stacks with small interface changes.

**SkyRL (RL rollout).** ThunderAgent is integrated into upstream SkyRL [3]’s main repository under `examples/train/thunder_agent` with an example training recipe at: [https://github.com/NovaSky-AI/SkyRL/tree/main/examples/train/thunder\\_agent](https://github.com/NovaSky-AI/SkyRL/tree/main/examples/train/thunder_agent). This recipe uses THUNDERAGENT as a rollout gateway for SkyRL training. Each agent trajectory is exposed to THUNDERAGENT as a program through a `program_id`, and the program is explicitly released after termination, matching the minimal interface described in Appendix B. The released recipe trains Qwen3-32B on R2EGym with SkyRL’s fully asynchronous framework and achieves a  $3.01\times$  wall-clock speedup over the baseline, demonstrating that THUNDERAGENT can be adopted in an existing agentic RL stack with minimal interface changes.

**NVIDIA Dynamo (serving).** As part of Dynamo 2.0<sup>3</sup>, THUNDERAGENT is being integrated into NVIDIA Dynamo<sup>4</sup>, a datacenter-scale distributed inference serving framework, to improve throughput for agentic inference workloads. The program abstraction proposed in THUNDERAGENT is standardized as part of the `nvext.agent_context`<sup>5</sup> serving protocol, operating as a first-class scheduling unit in Dynamo.

<sup>3</sup><https://github.com/ai-dynamo/dynamo/issues/9208>

<sup>4</sup><https://github.com/ai-dynamo/dynamo/pull/9448>

<sup>5</sup><https://github.com/ai-dynamo/dynamo/pull/8789>

## B System Portability and Interface Abstraction.

### B.1 Middleware Architecture and Unified Interfaces.

THUNDERAGENT serves as a **program-aware runtime layer** that mediates between agent control flow and backend inference engines via a program-level abstraction. The scheduler controls program state transitions based on the abstracted `ProgramState` (see Table 4a) together with the backend cache capacity view (see Table 5). Meanwhile, each program binds only to the endpoint and does not depend on the concrete backend implementation.

### B.2 Why program ID matters.

While the standard `session ID` serves as a routing label, **the program ID is used by our system to check the workflow metadata**. This visibility is critical: it allows the scheduler to distinguish valid tool-wait times from idle sessions, enabling smart preemption strategies that session-based baselines cannot support.

Only inference backend (e.g., vLLM/SGLang)

```

1 # 1) LLM request
2 chat_completion(model_id, messages, extrabody)
3
4 # 2) Tool execution
5 run_tool(command, sandbox)
6
7 # 3) Program end
8 # (no explicit release)

```

With ThunderAgent

```

1 # 1) LLM request
2 extrabody["program_id"] = "PID"
3 chat_completion(model_id, messages, extrabody)
4
5 # 2) Tool execution
6 run_tool(command, sandbox, program_id="PID")
7
8 # 3) Program end (explicit release)
9 POST /programs/release
10 { "program_id": "PID" }

```

Figure 11: Only three changes are required to use the ThunderAgent.

### B.3 Low-overhead adoption of the ThunderAgent.

Figure 11 shows that adopting ThunderAgent **only requires** attaching `program_id` to requests (for both LLM inference and tool execution) and sending an explicit release signal with `program_id` when a program ends. The `program_id` tags each request with its own program instance for scheduling, while the release signal allows ThunderAgent to reclaim per-program resources after termination. **All other request fields and the OpenAI-style API surface remain unchanged.**

Field	Type	Meaning	Status	Meaning
<b>ProgramState</b>			<b>ProgramStatus</b>	
<code>status</code>	<code>ProgramStatus</code>	Current lifecycle state.	<code>REASONING</code>	On-GPU inference.
<code>backend_url</code>	<code>str</code>	Assigned backend endpoint.	<code>ACTING</code>	Off-GPU tool exec.
<code>step_count</code>	<code>int</code>	Executed steps so far.	<code>PAUSED</code>	In global paused waiting set.
<code>total_tokens</code>	<code>int</code>	Total tokens over full history.	<code>STOPPED</code>	Released; resources reclaimed.

(a) ProgramState fields.

(b) ProgramStatus semantics.

Table 4: Program state and status definitions.

Field	Type	Meaning
<b>BackendState</b>		
url	str	Backend endpoint.
healthy	bool	Health flag for scheduling.
cache_config	Optional[CacheConfig]	Static cache configuration (fetched at startup).
active_program_tokens	int	Active token footprint on this backend.

Table 5: Key fields of BackendState.

## C Tool execution time variability.

**Practical agent tool calls are hard to characterize and often unpredictable.** In some code-centric settings (e.g., serving SWE-Bench [10] with SWE-agent [28] or OpenHands [24]), agents primarily invoke local, lightweight tools, and tool latency is relatively stable with low variance. However, in broader and more realistic scenarios, e.g., serving HLE [16] with ToolOrchestra [19], the workload relies more heavily on remote-service tools (Table 6), making tool execution time volatile and difficult to predict. This volatility largely stems from factors external to the agent runtime, such as network jitter, backend load and queuing delays, and rate limiting, which can vary across requests and over time.

We empirically confirm this behavior in Figure 12. For remote-service tools (and some execution tools), the gap between the median and tail quantiles is large: p95 and p99 are substantially higher than the median, and the tail can extend to tens or even hundreds of seconds. This suggests that tool latency in these settings lacks a stable central tendency; instead, heavy-tailed behavior dominates, **making tool latency prediction intrinsically brittle in practice.**

Given the unpredictability of tool execution, underestimation wastes pinned cache capacity while still triggering premature KV eviction, causing thrashing upon resume. Overestimation, in contrast, may lead to unnecessary eviction of programs’ KV that should have remained pinned. Even if tool runtimes were perfectly predictable, existing methods such as continuum [12] still decide whether to keep the KV cache pinned using a static, threshold-based rule. In contrast, ThunderAgent builds **a complete cost-modeling framework** and **dynamically trades off**  $Cost_{\text{recompute}}$  and  $Cost_{\text{caching}}$ .

Tool bucket	Role	Primary variability source
HLE-search	Retrieve evidence	Remote service(Network latency/Rate limits)
HLE-enhance-reasoning	Model-as-a-tool call	Remote service
HLE-answer	Final generation	Local LLM inference
SAB-execute_bash	Shell execution	Sandbox and I/O
SAB-execute_ipython_cell	Python cell execution	Program runtime
SAB-str_replace_editor	File edit	Local filesystem
SAB-task_tracker	Task state tracking	Local filesystem

Table 6: Tool buckets.

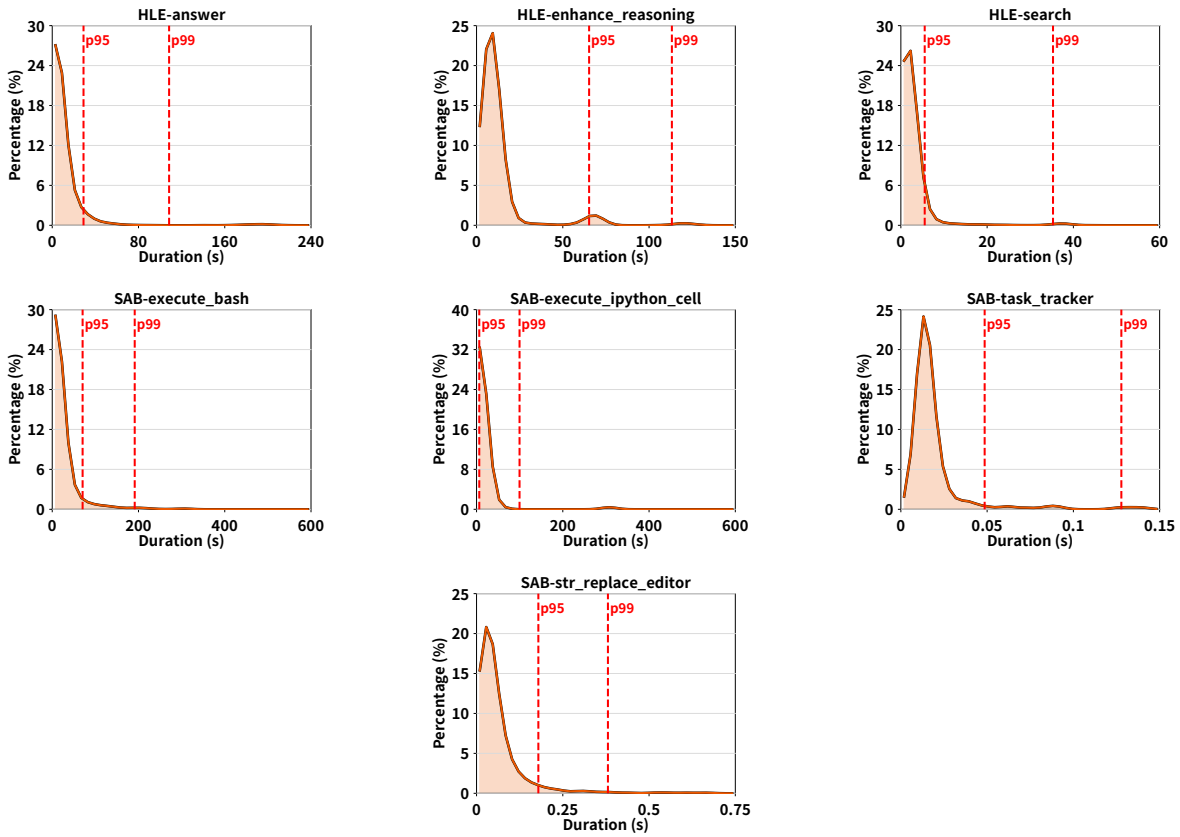


Figure 12: **Tool execution time distributions.** Tool execution time exhibits high variability and is difficult to predict.

## D KV cache hit rate statistics and interpretation

In our cost decomposition Equation (3), throughput loss in agentic serving mainly comes from *non-productive* overheads: KV re-computation induced by thrashing and idle KV caching during external tool execution, i.e.,  $\text{Cost}_{\text{recompute}}$  and  $\text{Cost}_{\text{caching}}$ . When tool calls are short and predictable, the acting phase occupies KV for only a short time, so  $\text{Cost}_{\text{caching}}$  is small; thus, avoiding thrashing dominates: a higher KV cache hit rate typically implies fewer re-prefills and higher throughput.

However, when tool execution times are highly variable (see Appendix C), a TTL-based scheduler can end up pinning the KV for long tool calls. While this can reduce  $\text{Cost}_{\text{recompute}}$  and thus increase the KV cache hit rate, it simultaneously inflates  $\text{Cost}_{\text{caching}}$  and reduces throughput. This helps explain why continuum [12] can underperform on tool-heavy workloads despite achieving a higher KV cache hit rate (Figs. 4, 5).

**ThunderAgent adapts to these regimes by explicitly balancing caching and recomputation.**

ThunderAgent introduces a time-decay function  $f(t)$  in Sec. 4.3 for acting programs to trade off  $\text{Cost}_{\text{caching}}$  and  $\text{Cost}_{\text{recompute}}$ ; we rigorously derive the optimal functional form of  $f(t)$  in Appendix F.1. By progressively lowering the effective memory priority of long-idle acting programs, the scheduler evicts their KV caches to reduce idle caching cost while controlling recomputation, yielding better throughput in practice (Figs. 4).

## E End-to-End Latency Analysis

Though we have stated in Section 1 that program-level latency (time used for whole workflow generation) is far more important than end-to-end per step latency for autonomous agents and agentic RL rollout. Here we compare THUNDERAGENT’s average per-step latency with vLLM and Continuum. Figure 13 shows that THUNDERAGENT significantly outperforms vLLM and Continuum when applying GLM4.6 and Qwen3 235B with mini-SWEAgent and Openhands on a single H100 serving in either low or high parallel workflow number. **The reason is that it seems to improve end-to-end latency by switching acting programs. But it actually delays all the running programs’ latency by triggering heavy KV-cache thrashing.**

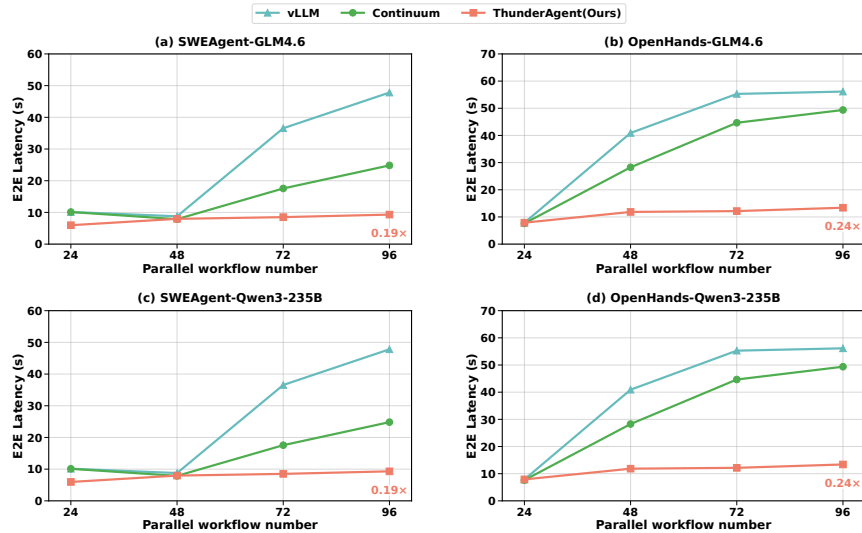


Figure 13: End-to-End latency comparison

## F Extended Theoretical Analysis.

### F.1 Proof of Time Decay Function for Periodic Thrashing Detection.

**Hypothesis F.1** (Unpredictable Tool Execution Time). *For acting programs, we hypothesize that the scheduler cannot reliably predict the tool return time for a given program (see Appendix C). Consequently, the decay function  $f$  should depend only on the elapsed acting time  $t$  in a time-homogeneous manner [15].*

**Hypothesis F.2** (Boundary Conditions). *We assume the time decay function  $f : [0, \infty) \rightarrow (0, 1]$  satisfies*

$$f(0) = 1, \lim_{t \rightarrow \infty} f(t) = 0, \quad (12)$$

*An intuitive interpretation of these boundary conditions is that, when the tool execution time is 0, corresponding to a multi-turn interaction without tool calls, all acting programs reduce to reasoning programs, and therefore  $f(t) = 1$ . Conversely, if the tool execution time is infinite, the agentic workflow collapses to single-turn generation, akin to standard chatbot serving, since requests never return for the next-turn interactions. In this regime, setting  $f(t) = 0$  aligns the decay function with request-level scheduling policies.*

**Theorem F.1** (Admissible Time Decay Functions). *Under Hypothesis F.1 and F.2, the admissible time decay function  $f$  for our capacity check function in Equation 7 must take one of the following forms: exponential in continuous time,  $f(t) = e^{-\lambda t}$  with  $\lambda > 0$ , or geometric in discrete tick time,  $f(k) = x^{-k}$  with  $x > 1$ .*

*Proof.* We prove this theorem by first formalizing the time-homogeneous property implied by Hypothesis F.1. Next, we inducing the admissible time decay functions  $f$  under the boundary conditions in Hypothesis F.2.

**Formalization of unpredictable tool time.** Let  $t$  denote the elapsed acting time, measured in wall-clock time (continuous time) or in periodic-monitor ticks (discrete time). Under Hypothesis F.1, the relative decay after waiting an additional duration  $\Delta$  should not depend on the absolute elapsed time  $t$ , but only on the increment  $\Delta$ . We formalize this as the existence of a function  $\phi : [0, \infty) \rightarrow (0, 1]$  such that, for all  $t, \Delta \geq 0$ ,

$$f(t + \Delta) = f(t) \phi(\Delta). \quad (13)$$

**Semigroup equation.** Setting  $t = 0$  in Equation 13 and using the boundary condition  $f(0) = 1$  (from Hypothesis F.2) yields  $\phi(\Delta) = f(\Delta)$ . Substituting back, we obtain the multiplicative semigroup equation

$$f(t + \Delta) = f(t) f(\Delta), \quad \forall t, \Delta \geq 0. \quad (14)$$

**Continuous-time case (exponential decay).** We first consider the continuous-time case. Define  $h(t) \triangleq \ln f(t)$ . Applying the logarithms on both sides of Equation 14 yields the *Cauchy functional equation*

$$h(t + \Delta) = h(t) + h(\Delta). \quad (15)$$

Since  $f(t) \in (0, 1]$ , we have  $h(t) \leq 0$  for all  $t \geq 0$ , which implies that  $h$  is bounded above on  $[0, \infty)$ . Under this boundedness condition, the Cauchy functional equation admits only linear solutions of the form  $h(t) = ct$  for some  $c \in \mathbb{R}$ . Writing  $\lambda \triangleq -c \geq 0$ , we obtain

$$f(t) = e^{-\lambda t}. \quad (16)$$

Finally, the boundary condition  $\lim_{t \rightarrow \infty} f(t) = 0$  (Hypothesis F.2) rules out  $\lambda = 0$ , and thus  $\lambda > 0$ .

**Discrete-time case (geometric decay).** We next consider the discrete-time setting, where elapsed acting time is measured in integer ticks  $k \in \mathbb{Z}_{\geq 0}$ . Equation 14 becomes

$$f(m + n) = f(m) f(n), \quad \forall m, n \in \mathbb{Z}_{\geq 0}. \quad (17)$$

Setting  $n = 1$  yields the recurrence  $f(k) = f(k - 1) f(1)$ . Let  $\gamma \triangleq f(1)$ , we have  $f(k) = f(1)^k \triangleq \gamma^k$ . The boundary condition  $\lim_{k \rightarrow \infty} f(k) = 0$  implies  $0 < \gamma < 1$ . Equivalently, we can parameterize

$$f(k) = x^{-k}, \quad x \triangleq \gamma^{-1} > 1. \quad (18)$$

This completes the proof. □

## F.2 Proof of recomputation STP cost

As defined in Section 4.2, the STP recomputation cost is given by:

$$\text{Cost}_{\text{recompute}} = \int_0^{t_{\text{recompute}}} c_i(t) dt \quad (19)$$

where  $c_i(t)$  represents the instantaneous cost, which is proportional to the decoding step (i.e.,  $c_i(t) \propto t$ ). This proportionality arises because chunked prefill processes a constant number of KV pairs per iteration, resulting in a linear increase in accumulated computation over time. Consequently, evaluating the integral yields  $\text{Cost}_{\text{recompute}} \propto t_{\text{recompute}}^2$ . Given the relationship  $t_{\text{recompute}} = c_i \times T_{\text{decode}}/\text{chunk}$ , where both  $T_{\text{decode}}$  and the chunk size are constant, it follows that:

$$\text{Cost}_{\text{recompute}} \propto c_i^2$$

## F.3 Proof of minimized recomputation STP cost

We provide a rigorous proof for the optimality of the Shortest-First Eviction policy using an **exchange argument**.

**Problem Definition.** We aim to select a subset of paused programs  $S$  to evict such that the total reclaimed memory satisfies  $\sum_{i \in S} c_i \geq \Delta C$ , while minimizing the total re-computation cost  $J(S) = \sum_{i \in S} c_i^2$ . Note that the cost function  $f(x) = x^2$  is strictly convex and super-additive (i.e.,  $(a+b)^2 > a^2 + b^2$  for positive  $a, b$ ).

**Theorem.** The optimal strategy to minimize  $J(S)$  is to strictly select programs with the smallest context lengths  $c_i$ .

**Proof.** Suppose, for the sake of contradiction, that the optimal set  $S^*$  is *not* the set of the shortest programs. This implies there exists a "long" program  $p_{\text{long}} \in S^*$  and a "short" program  $p_{\text{short}} \notin S^*$  (available but not selected) such that  $c_{\text{short}} < c_{\text{long}}$ .

We can construct a new set  $S'$  by swapping or decomposing  $p_{\text{long}}$ . Since  $c_{\text{long}} > c_{\text{short}}$ , we can conceptualize  $p_{\text{long}}$  as being composed of a segment of length  $c_{\text{short}}$  and a residue  $r = c_{\text{long}} - c_{\text{short}}$ .

Replacing the selection of  $p_{\text{long}}$  with  $p_{\text{short}}$  (and theoretically the residue  $r$ ) changes the cost. Consider the inequality derived from the convexity of the square function:

$$c_{\text{long}}^2 = (c_{\text{short}} + r)^2 = c_{\text{short}}^2 + r^2 + 2c_{\text{short}}r \quad (20)$$

Since  $c_{\text{short}} > 0$  and  $r > 0$ , the cross-term  $2c_{\text{short}}r > 0$ . Therefore:

$$c_{\text{short}}^2 + r^2 < c_{\text{long}}^2 \quad (21)$$

This inequality implies that breaking a large eviction target ( $c_{\text{long}}$ ) into smaller components ( $c_{\text{short}} + r$ ) strictly reduces the sum of squares. In the context of our scheduler, this means that if we are satisfying the memory constraint  $\Delta C$  using a large program, we can strictly decrease the penalty by swapping it for available smaller programs (or a combination thereof) that sum to the same capacity.

By iteratively applying this exchange—replacing the largest selected programs with smaller unselected programs—we monotonically decrease the cost function  $J(S)$ . The cost reaches its global minimum only when no such exchange is possible, i.e., when  $S$  consists entirely of the programs with the smallest available context lengths.

**Conclusion.** The Shortest-First strategy is globally optimal because the super-linear cost of attention ( $O(L^2)$ ) penalizes fragmentation less than aggregation.

## G Additional Ablation Studies

We provide additional ablation studies that isolate the contribution of THUNDERAGENT’s individual design decisions, complementing the parameter-sensitivity ablation in [Section 5.4](#).

### G.1 Global vs. Local Waiting Queue

We compare THUNDERAGENT’s **global** waiting queue, which permits paused programs to be restored on a different DP node from their original backend, against a **local** waiting queue that always restores a program to its origin node. In the local variant, programs that pause on memory-saturated nodes must wait until their original node has capacity, whereas the global queue redistributes them to under-utilized peers.

As shown in [Figure 14](#), the global queue consistently improves throughput as we scale from 2 to 4 H100 nodes. At 4 nodes, the gain widens to 1.28 $\times$ , reflecting that cross-node memory imbalance grows with cluster size ([Figure 2a](#)); the global queue directly mitigates this imbalance.

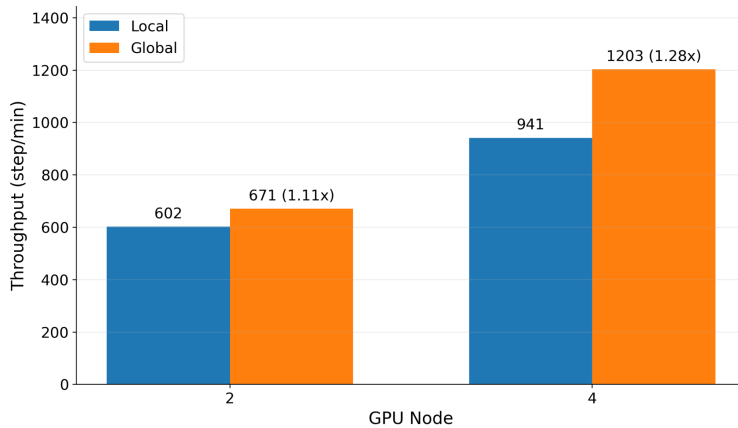


Figure 14: **Global vs. local waiting queue** on GLM-4.5-fp8 + mini-SWEAgent (8xH100 GPU, 72 concurrent programs per node).

### G.2 Time-Decay Function Form

[Theorem F.1](#) establishes that exponential decay is the unique admissible form of  $f(t)$  under the unpredictable-tool-latency assumption and the boundary conditions in [Hypothesis F.2](#); we now empirically compare it against two practical alternatives: **constant** ( $f(t) = 1$ , i.e., no decay), **linear** ( $f(t) = \max(1 - t, 0)$ ), and **exponential** ( $f(t) = e^{-t}$ ). We evaluate on three agentic pipelines with progressively less predictable tool latency: mini-SWE-Agent (short, regular tool calls), OSWorld (longer but largely periodic tool calls, e.g., a fixed 5s interval between screenshots), and ScienceAgent (highly stochastic, heavy-tailed tool calls; see [Appendix C](#)).

As shown in [Figure 15](#), exponential decay is the most robust choice overall: it outperforms both alternatives on mini-SWE-Agent (1.08 $\times$ ) and ScienceAgent (1.63 $\times$  vs. 1.39 $\times$  for linear), where unpredictable or long-tailed tool latency exposes the brittleness of a static  $f(t)$ . On OSWorld, however, exponential decay trails linear by about 6% (1.14 $\times$  vs. 1.21 $\times$ ): when tool durations are themselves near-deterministic, a linearly shrinking weight tracks the predictable tool clock more tightly. Constant decay, which never reclaims memory from long-idle acting programs, is the weakest on every workload that exhibits any waiting at all.

### G.3 Eviction Policy

We empirically validate the shortest-first eviction policy proved optimal in Section F.3 against two natural baselines: **random** eviction and **longest-first** eviction. We run on two agentic pipelines, mini-SWE-Agent (*SWE*) and OpenHands, both with GLM-4.5-fp8 on a single H100 node at 72 concurrent programs.

As predicted by the  $O(L^2)$  recomputation cost (Section F.2), evicting the longest paused programs is the worst choice: the dropped KV state is the most expensive to rebuild on resume, inflating average prefill time and starving the decoding stream. Shortest-first achieves the highest throughput and the lowest average prefill time on both pipelines (Figure 16). The gap is largest on OpenHands, where program contexts are heaviest – shortest-first is roughly  $2.0\times$  the throughput of longest-first and cuts average prefill time by  $2\times$  (7.5 s vs. 15.1 s). Random falls between the two, consistent with it being an unbiased estimator over the same cost surface.

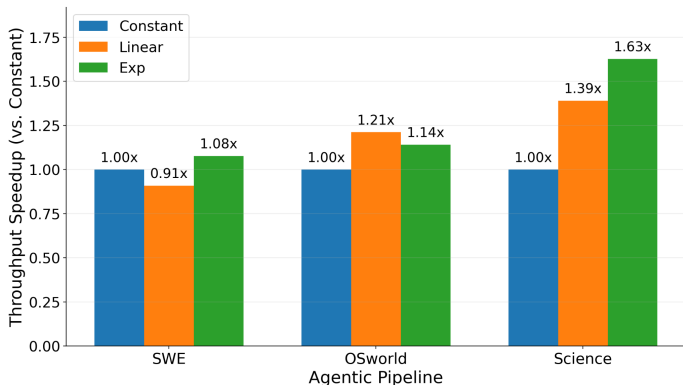


Figure 15: **Ablation of the decay function  $f(t)$**  across three agentic pipelines. Throughput is reported as speedup vs. the constant (no decay) baseline. Exponential decay is the most robust overall; linear decay is preferable only on OSWorld, where tool execution time is near-deterministic. Experiments are conducted on an 8xH100 node with 72 concurrent programs using GLM-4.5-fp8 model.

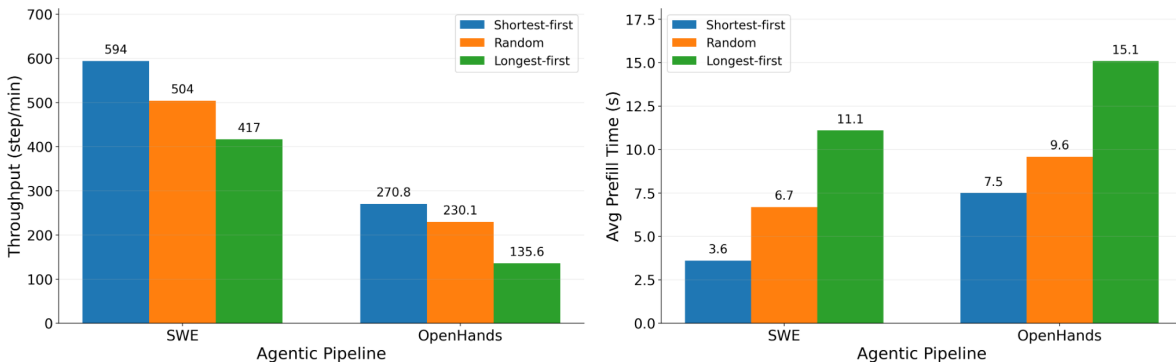


Figure 16: **Ablation of the eviction policy.** (Left) throughput, (right) average prefill time. Shortest-first eviction wins on both axes, with the gap widening on the heavier-context OpenHands pipeline. Experiments are conducted on an 8xH100 node with 72 concurrent programs using GLM-4.5-fp8 model.

## G.4 Component-wise Contribution

We disentangle the contribution of THUNDERAGENT’s two main scheduling components by starting from vanilla vLLM and incrementally enabling **local program-aware scheduling** (the cost-driven eviction + decay function operating per backend) and then the **global waiting queue** (cross-node program migration). Table 7 reports throughput on 2×H100 nodes with GLM-4.5-fp8 + mini-SWEAgent at 144 concurrent programs.

The largest jump comes from local program-aware scheduling, which raises throughput from 375 to 602 steps/min (1.61×) by directly suppressing unnecessary recomputation and idle caching cost (Equation 3) within each backend. Layering the global waiting queue on top adds a further 1.12× (602 → 672) by reducing cross-node memory imbalance, consistent with the standalone global-vs-local result in Section G.1.

Component	Throughput (steps/min)
vLLM (baseline)	375
+ local program-aware scheduling	602
+ global waiting queue (THUNDERAGENT)	672

Table 7: Component-wise ablation on 2×H100 + GLM-4.5-fp8 + mini-SWEAgent at 144 concurrent programs. Speedups are reported against vLLM. Local scheduling delivers the majority of the gain; the global queue is responsible for the remaining cross-node imbalance reduction.